# COMPUTATIONAL PROPERTIES OF URANIUM-ZIRCONIUM

A Thesis
Presented to
The Academic Faculty

by

Alex Moore

In Partial Fulfillment
of the Requirements for the Degree
Masters of Science in the
School of Mechanical Engineering

Georgia Institute of Technology
December 2013

# COMPUTATIONAL PROPERTIES OF URANIUM-ZIRCONIUM

Approved by:

Dr. Chaitanya S. Deo, Advisor
School of Mechanical Engineering
*Georgia Institute of Technology*

Dr. Weston M. Stacey, Jr.
School of Mechanical Engineering
*Georgia Institute of Technology*

Dr. Yan Wang
School of Mechanical Engineering
*Georgia Institute of Technology*

Date Approved: 10/21/2013

# ACKNOWLEDGEMENTS

To Idaho National Laboratory for their Financial support. Thank you to my family and friends for their continued support.

# TABLE OF CONTENTS

# LIST OF TABLES

# LIST OF FIGURES

Page

# LIST OF SYMBOLS

**Ensemble Notation**

| | |
|---|---|
| $\langle A \rangle$ | Generic Ensemble Property Average |
| $A_i$ | Generic Property of State i |
| $\beta$ | Reduced Temperature |
| E | Total Energy |
| H | Enthalpy |
| L | Hill Energy |
| $\mu$ | Chemical Potential |
| N | Number of Moles |
| $p_i$ | Probability of state i |
| P | Pressure |
| t | Time |
| T | Temperature |
| U | Potential Energy |
| V | Volume |
| Z | Partition Function |

**Simulation Notation**

| | |
|---|---|
| $\alpha$ | Energy Minimization Multiplication Factor |
| $\Delta E$ | Change in Energy |
| F | Force |
| $k_B$ | Boltzmann's Constant |

| | |
|---|---|
| m | Mass |
| $P_{XY}$ | Probability Transformation from State X to Y is Accepted |
| $r_{max}$ | Maximum MC Displacement Distance |
| r | Position |
| T | Temperature |
| U | Potential Energy |

**Analysis Notation**

| | |
|---|---|
| $\alpha_V$ | Volumetric Thermal Expansion |
| B | Bulk Modulus |
| C | Elastic Constants |
| $C_{44}$ | Shear Modulus |
| $C_{12}$ | Transverse Expansion Elastic Constant |
| C' | Shear Zener Constant |
| ε | Strain |
| E | Modulus of Elasticity |
| $E_V$ | Vacancy Formation Energy |
| En | Energy of the pure Crystal |
| $E_i$ | Interstitial Formation Energy |
| G | Gibbs Free Energy |
| g(r) | Radial Distribution Function |
| H | Enthalpy |
| $k_B$ | Boltzmann's Constant |
| N | Number of Atoms |

| | |
|---|---|
| $n_A$ | Atomic Fraction of A Type Atoms in the Entire System |
| p or P | Pressure |
| $P_{AA}$ | Fraction of Nearest Neighbor Sites of Atom Type A Occupied by A Type Atoms |
| $\rho_0$ | Average Density of the System |
| r | Distance |
| S | Entropy |
| $\sigma$ | Short Range Order (SRO) |
| $\sigma$ | Stress (Elastic Theory) |
| T | Temperature |
| U | Internal Energy |
| V | Volume |

**DFT Notation**

| | |
|---|---|
| E | Total Energy |
| $E_{xc}$ | Exchange Correlation Functional |
| $E_{xt}$ | Electron-Ion Coulombic Interaction |
| $E_{ii}$ | Ion-Ion Energy |
| J | Hartree Electron-Electron Energy |
| N | Number of Electrons |
| $\rho$ | Electron Density |
| $\psi$ | Wave Function |
| Ts | Single Particle Kinetic Energy |
| U | Potential Energy |
| $\vec{x}$ or $\vec{r}$ | Position |

**MEAM Notation**

| | |
|---|---|
| A | Adjustable MEAM Parameter |
| a | Ratio Between 2NN Distance and 1NN Distance |
| a* | Temporary UBER Variable |
| alat | Adjustable MEAM Parameter for Lattice Constant |
| $\alpha$ | Adjustable MEAM Parameter |
| B | Bulk Modulus |
| $\beta^{(h)}$ | Adjustable MEAM Parameters of the Partial Electron Density Decay |
| C | Screening Ellipse Parameter |
| $C_{min}$ | Adjustable MEAM Parameter for the Minimum Ellipse Screening Parameter |
| $C_{max}$ | Adjustable MEAM Parameter for the Maximum Ellipse Screening Parameter |
| $\Gamma$ | Intermediate Electron Density Term |
| $\delta$ | Adjustable MEAM Parameter – Cubic Attraction/Repulsion Term |
| $\Delta_{ij}$ | Adjustable MEAM Parameter for the Alloy Cohesive Energy Adjustment |
| Ec | Cohesive Energy |
| $E^u$ | Universal Function for the Universal Binding Energy Relationship (UBER) |
| F | Embedding Function |
| $f_C$ or $f_{CUT}$ | Cut-off Function |
| lat | MEAM Reference Structure |
| $P_l^0$ | Legendre Polynomials |
| $\rho^a$ | Atomic Electron Density |
| $\rho$ | Electron density |

| | |
|---|---|
| $\rho^e$ or $\overline{\boldsymbol{\rho^0}}$ | Background Electron Density of the Reference Structure |
| $\rho_i^{(i)}$ | Partial Background Electron Densities |
| $\rho_0$ | Electron Density Scaling Factor |
| $\rho_e$ | Reference Structure Equilibrium Electron Density |
| $R_{ij}$ | Distance Between Atoms i and j |
| $R_{cut\text{-}off}$ | Cut-Off Distance for the MEAM Potential |
| r | Position |
| $r_e$ | Reference Structure Equilibrium 1NN Distance |
| S | Screening Function |
| $t^{(l)}$ | Adjustable MEAM Parameter for Partial Electron Density Weighting Factors |
| $\phi$ | Pair Potential |
| U | Potential Energy |
| x | Temporary Screening Variable |
| xncut | Power Coefficient in Cut-off Function |
| xmcut | Power Coefficient in Cut-off Function |
| y | Temporary Screening Variable |
| $\psi$ | Temporary Pair Potential |
| $Z_1$ | Number of 1NN Atoms |
| $Z_2$ | Number of 2NN Atoms |
| $\Omega$ | Volume per Atom in the Reference Structure |

# SUMMARY

The metallic binary-alloy fuel Uranium-Zirconium is important for use in the new generation of advanced fast reactors. Uranium-Zirconium goes through a phase transition at higher temperatures to a (gamma) Body Centered Cubic (BCC) phase. The BCC high temperature phase is particularly important since it corresponds to the temperature range in which the fast reactors will operate. A semi-empirical Modified Embedded Atom Method (MEAM) potential is presented for Uranium-Zirconium. This is the first interatomic potential created for the U-Zr system. The bulk physical properties of the Uranium-Zirconium binary alloy were reproduced using Molecular Dynamics (MD) and Monte Carlo (MC) simulations with the MEAM potential. The simulation of bulk metallic alloy separation and ordering phenomena on the atomic scale using iterative MD and MC simulations with interatomic potentials has never been done before. These simulations will help the fundamental understanding of complex phenomena in the metallic fuels. This is a large step in making a computationally acceptable fuel performance code, able to replicate and predict fuel behavior.

# CHAPTER 1

## INTRODUCTION

Since the Clementine reactor in 1949, the first nuclear fast reactor, metal alloy fuels have interested the nuclear community, and a number of experimental fast reactors have employed nuclear metallic fuel, including the EBR series, LAMPRE series, DFR and the Fermi reactors (Kittel 1993).

Generally ceramic nuclear fuel is used in the Light Water Reactors (LWR) and Pressurized Water Reactors (PWR); however, recently there has been increased research in using metallic fuels in a LWR (Malone 2012). Metallic fuels have already been shown to have many benefits when used in non-water cooled reactors. Initially metallic fuels were used for their ease of fabrication, high heavy metal density and favorable breeding efficiencies, but recently they are being noticed for additional significant benefits. Metal alloy fuels demonstrate superior performance over ceramic fuels in that they behave in a benign manner during core off-normal events; maintain integrity in high burn-up conditions; and have low-loss fuel recycling during reprocessing. They also have proliferation-resistant recycling, a high thermal conductivity, passive reactor safety, and fairly isotropic neutron cross-sections. (Kittel 1993; Olander 1975)

### Metallic Fuel Advantages

Nuclear metallic alloy fuels are believed to have a very promising future in the new advanced fast reactor designs and research for several reasons. First, they do not require plutonium to be separated during reprocessing, which is a benefit in regard to national security threats. One of the largest concerns for nuclear national security is terroristic efforts to obtain material in order to create a nuclear device. However, the

metallic fuel reprocessing, as opposed to ceramic fuel reprocessing, would ensure that key isotopes and elements required for a supercritical nuclear device would not have to be separated from the bulk and therefore could not be a target or opportunity for terroristic efforts. Another benefit is that reprocessing of metallic fuel allows for reduced fuel cycle cost.

Secondly, the metallic fuels have the potential for the highest fissile atom density, resulting in a higher burn-up potential of nuclear fuel. This would allow reactors to operate longer before refueling; create an opportunity to breed more plutonium during reactor operation, resulting in high utilization of fuel resources; and allow for smaller reactors with a high power density.

Third, nuclear metallic alloy fuels have favorable thermodynamic properties, promoting safety and energy harvesting. They have a high thermal conductivity leading to lower fuel and cladding temperatures and less stored energy.

Metallic fuels also have favorable neutronic properties. At the reactor operating conditions, many of the metallic fuels are in the BCC phase resulting in very isotropic neutron cross-sections. These isotropic neutron cross sections are particularly important for small fast nuclear reactors.

Lastly, metallic fuels have passive safety features during core off-normal events. For example, during a loss-of-flow accident, fission gases and thermal expansion cause the fuel to expand to the cladding, whereupon the fuel at the fuel/cladding interface will transform to the molten phase, removing reactivity from the core.

There are some drawbacks to the use of metal alloy nuclear fuels as well. They have high fission gas release and swelling during irradiation and a lower melting point than the traditional ceramic nuclear fuels. They can also react with water. Nonetheless, some of these disadvantages have actually been realized to be beneficial. One of the disadvantages that can also be seen as a benefit is the low melting point. The low melting point allows for the fuel to go into the molten phase which reduces reactor reactivity,

acting as a passive safety feature (this process is described further in the Fuel Disadvantage Section below).

## Metallic Fuel Disadvantages

Each nuclear fuel type has its advantages and disadvantages, and no single fuel type will perform better than the others in all scenarios. There are a few concerns that need to be considered when using metallic fuels in particular, such as fuel swelling, fission gas release, fuel redistribution, cladding interactions and coolant interactions.

Fuel swelling and irradiation growth are drastic phenomena that metallic fuels undergo when irradiated. Swelling in the fuel means that the fuel maintains a similar shape but the volume increases, while irradiation growth means a change in shape with no noticeable change in volume. At the onset of operation, metallic fuels will swell rapidly due to fission gas bubbles until the bubbles become interconnected and make a path for the gas to escape. After the bubbles are interconnected, the swelling behavior of metallic fuels is very slow and is caused by the solid fission products taking up lattice positions in the fuel. The addition of the solid fission product accumulation leads not only to slow swelling, but also to a loss in thermal conductivity. Furthermore, grain boundary tearing at the fuel edges has been seen to cause large irregular shaped cavities. Both the irradiation growth and grain boundary tearing are known to result in reactivity loss (Pahl 1990).

The Fuel Cladding mechanical interaction (FCMI) is a large concern when using metallic fuels. As irradiation of the fuel progresses, the irradiation/thermal creep by fission gas pressure loading can eventually cause a stress-rupture of the cladding (Pahl 1990; Pahl 1992). Until the 1960's the burn-up of the metallic fuels in fast reactors was limited by the FCMI (Ogata 1996). A technical breakthrough from Argonne National Laboratory (ANL), drastically decreased the FCMI and allowed the burn-up potential of the metallic fuels to be realized (Walters 1984). Reducing the smear density down to

approximately 75% provided enough space for the fuel to swell inside the cladding until the fission gas pores became interconnected and fuel swelling due to fission gasses stopped.

Fuel-cladding chemical interactions (FCCI) must also be considered when using metallic fuels. The creep rupture at high burn-up is known to be accelerated by FCCI. Experiments have shown that there is fuel-cladding interdiffusion, in which Uranium, Plutonium, and some lanthanide fission products, react and can penetrate into the cladding. The result of this interdiffusion is cladding wall thinning, a brittle cladding layer between the fuel and cladding, and a eutectic composition approached in the fuel which causes a lower melting point in that region (Pahl 1990; Hayes 2009; Ogata 1997).

Another concern when using metallic fuels is the fuel constituent restructuring of Uranium and Zirconium have been experimentally witnessed in the U-Zr type metallic fuels. The Uranium and Zirconium redistribution occurs soon after reactor operation begins from U and Zr interdiffusion. However, the inhomogeneity associated with the restructuring, while changing some of the mechanical and neutronic properties of the fuel, has not noticeably affected the overall fuel lifetime, but a lowered solidus temperature has been noticed in some fuel regions (Pahl 1990; Kim 2004).

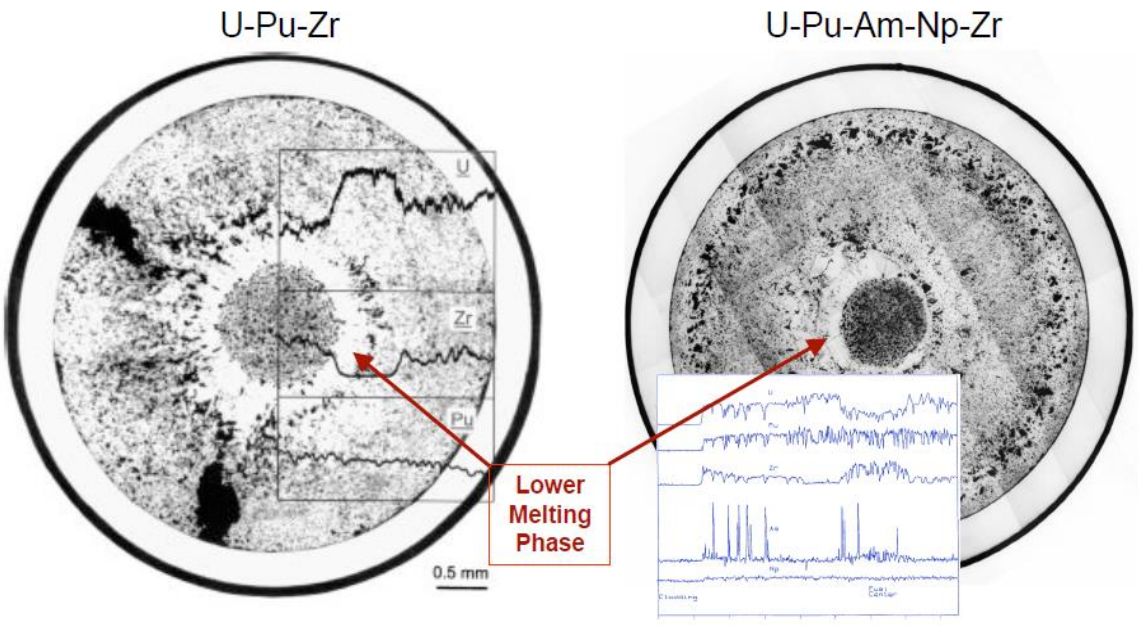


Figure 1: Post-irradiation Optical Metallography and Measured Constituent Redistributions (Kim 2004; Hofman 1996)

All nuclear metallic fuels have a lower melting temperature than the nuclear ceramic fuels. The solidus temperature for Uranium metals can be increased when alloyed to another metal with the same BCC high temperature phase. Common metals alloyed to Uranium are Zirconium, Niobium and Molybdenum. For reactor operation the fuels must be kept below their melting temperature. However, since the thermal conductivity of these metallic fuels is higher than that of the ceramic fuels, the heat flux from the fuel pin is higher, which leads to a lower temperature gradient across the fuel pin and allows for a high power density to be achieved while remaining below the fuel melting temperature. Nevertheless, this low melting temperature can cause problems during fast transients.

Depending on the fuel temperature and the Zirconium redistribution, the fuel could have multiple phases during reactor operation, causing changes in both mechanical and neutronic properties.

The swelling and low melting point of metallic fuels is a benefit during off-normal core events. The interconnected porosity of swollen metallic fuel coupled with the low melting point during a transient event allows for the thermal expansion of the fuel due to temperature induced phase transformations; this phase transformation prevents the fuel from stressing the cladding, and allows the fuel to flow onto itself in the open porosity (Ondracek 1973).

However, the metallic fuels still need additional research before they can be fully understood. One of the barriers obstructing the advancement of metallic fuels is the lack of appropriate tools needed for computational simulations. Computational simulation is a tool that can be used to give insight into physical phenomena resulting in overall mechanical and thermal properties that cannot be attained from experimentation alone. Computational simulation not only gives insight into experimental results, but also, once developed, allows for the necessary predictions of metallic fuel property changes under a variety of conditions which is needed when developing core models. In addition, computational simulation combined with experimentation will not only assist in the operation and design of a reactor, but also provide the necessary information and insights for optimizing fabrication and reprocessing of the fuels. Experimentation alone does not allow for the full picture of properties of the metallic fuels at high temperature to be seen. Experimentation at high temperature phases is also problematic: it is difficult to obtain accurate and reliable data due to severe thermal scatter.

## Uranium (U)

Uranium is a transition metal that has three distinct stable solid phases. The transition of these phases can be attributed to the behavior of the de-localized f orbital-electrons. The ground state Uranium phase is the α (orthorhombic) phase. As temperature increases Uranium will go through transitions to the β (tetragonal) and the γ (body centered cubic) phases respectively (Yoo 1998). The α and β phases of Uranium

have unwanted an-isotropy of expansion, but the γ phase has seemingly isotropic expansion which are desirable in reactor environments. Uranium's transition temperatures from α to β and from β to γ are 935K and 1045K respectively (Soderlind 1998).

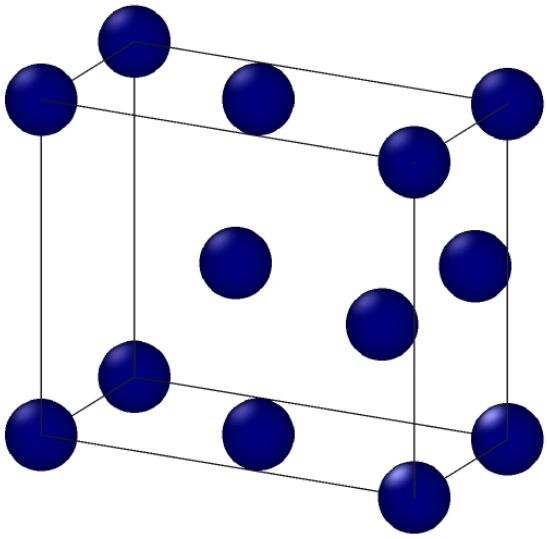

Figure 2: The Unit Cell of the α-U Crystal Structure

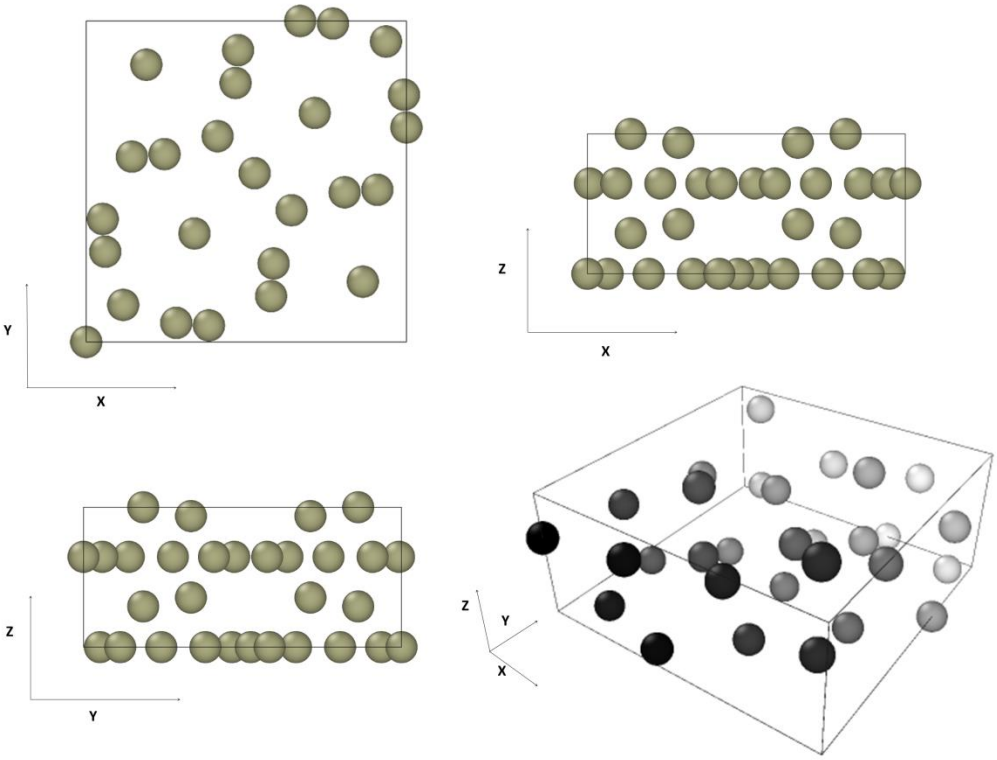


Figure 3: The β-U Crystal Structure (Beeler 2012a)

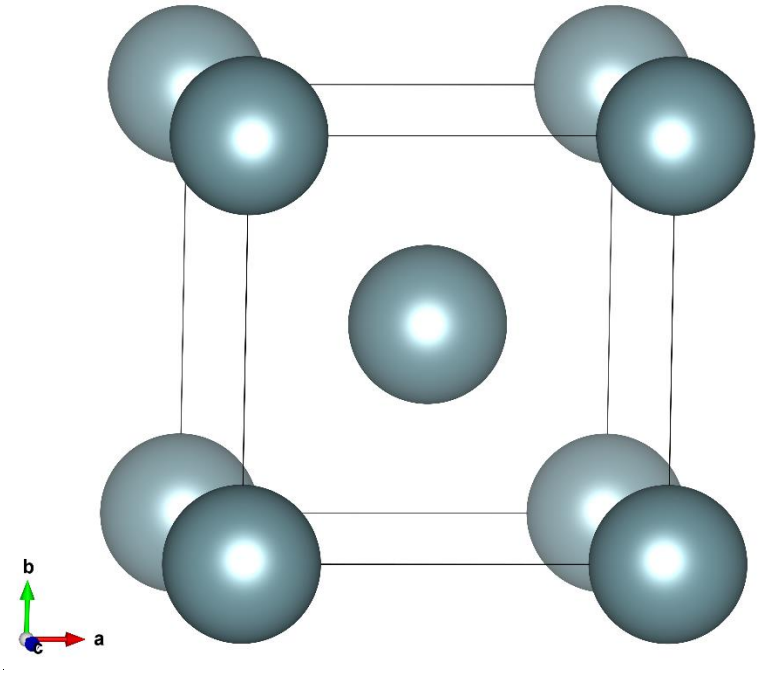


Figure 4: The γ-U Crystal Structure

**Zirconium (Zr)**

Zirconium is also a transition metal and has two distinct solid phases. The ground phase of Zirconium is hexagonally closed packed (hcp or αZr), while the high temperature phase is body centered cubic (bcc or βZr). The transition temperature from αZr to βZr occurs at 863 °C. Another important characteristic of Zirconium is its high melting point of 1855 °C, which makes Zirconium useful when alloying to Uranium as it raises the melting point of the alloy.

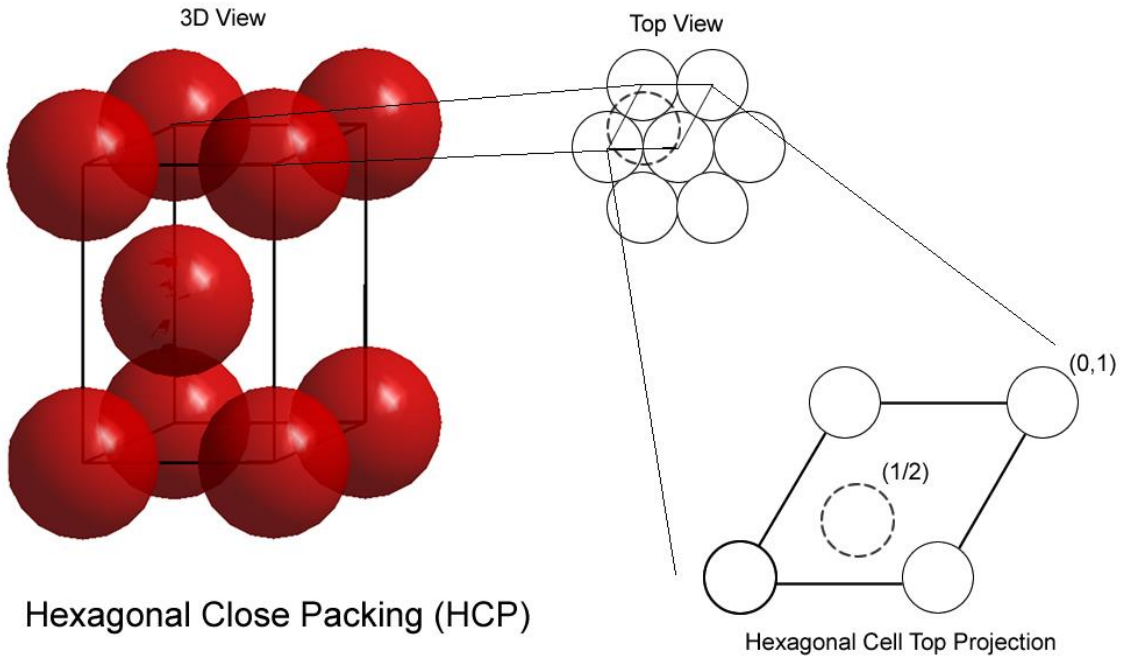


Figure 5: Unit cell of α-Zr Crystal Structure ("Hexagonal Closed Packing HCP")

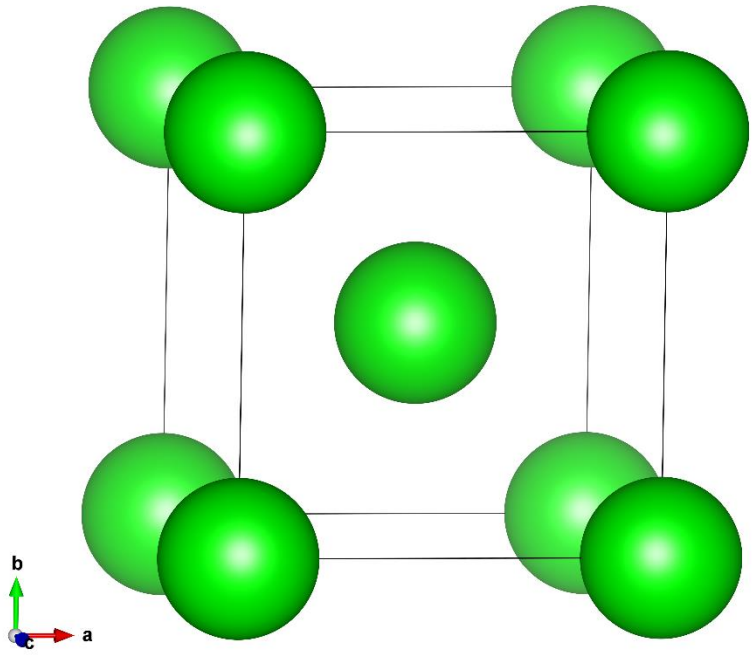


Figure 6: The β-Zr Crystal Structure

## Uranium-Zirconium (U-Zr)

Zirconium is one of the principal structural metals for fuel cladding and other core components because of its high temperature BCC phase (above 865ºC), high melting temperature, very low thermal neutron absorption cross-section, relatively low cost and high fission product yield. For these reasons it was considered a good option to alloy with Uranium to construct a metallic alloy fuel. However, the choice of which element to alloy to Uranium for a good metallic fuel has mostly been decided by trial and error, often making a compromise between mechanical properties and corrosion resistance. After many experiments and tests, Uranium-Zirconium (U-Zr), along with a few other alloys, appears to be a promising option as a nuclear fuel for fast reactors.

Uranium-Zirconium has a Body Centered Cubic (BCC) structure for reactor operating temperatures; therefore, the BCC structure is particularly important to analyze. It is also important to note that the Uranium-Zirconium alloy goes through a $\delta$ (C32 Crystal Structure) to $\gamma$ (BCC) phase transition for 65%-75% Zirconium around 890 Kelvin.

The most recent phase diagram was constructed by H. Okamoto (Okamoto 2007) and was made from a compilation of experimental papers on Uranium-Zirconium.

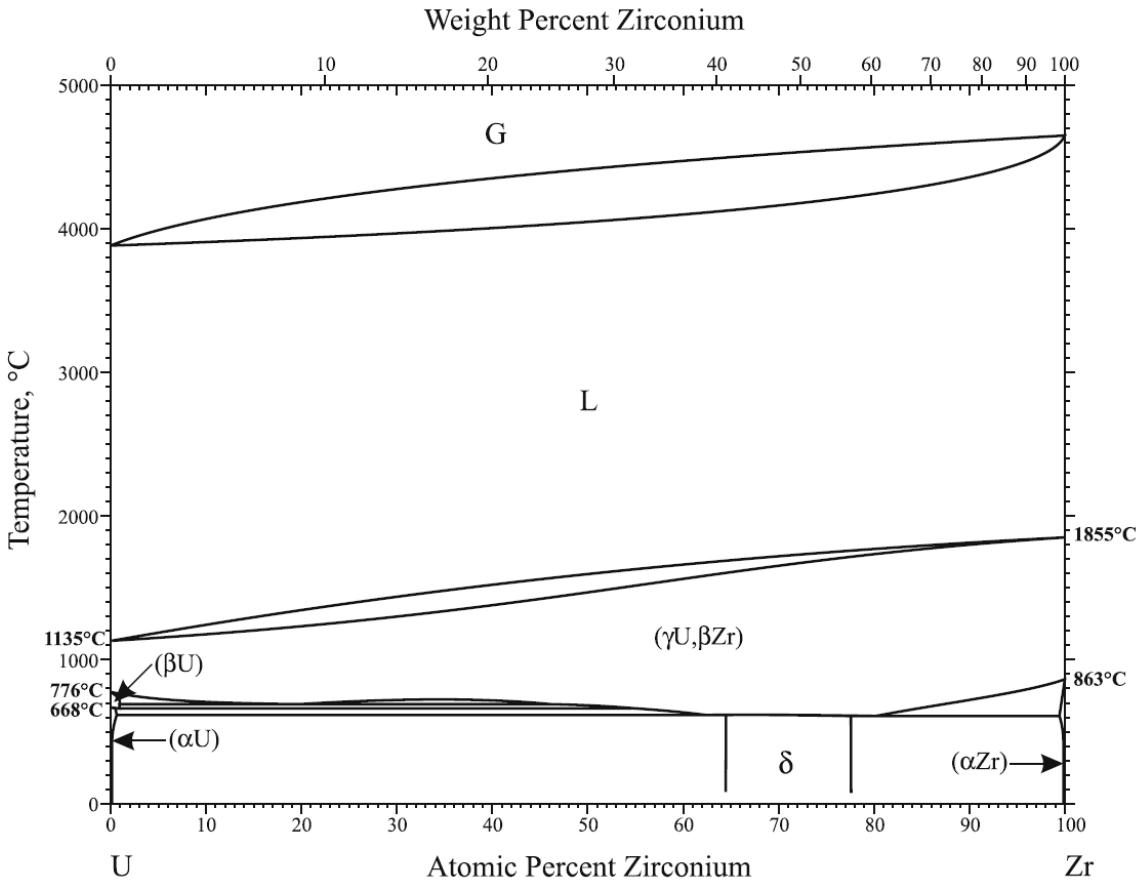


Figure 7: Phase Diagram of U-Zr (Okamoto 2007)

The γU, βZr phase is known to be completely miscible. This is the high temperature phase in which the metallic U-Zr fuel has isotropic properties and the main phase of interest for high temperature fast reactors.

Uranium-Zirconium (including U-Pu-Zr and U-ZrH) fuel is already considered to be one of the best options for use in the TRIGA pool type reactors and the Generation IV SFR's reactors (EBR-II, SABR, S-PRISM and more). Uranium-Zirconium in reactor operating conditions is in the Body Centered Cubic (BCC) phase. The BCC phase gives the metallic fuel the desired isotropic thermal expansion, but has less experimental data than the lower temperature phases. This research focuses on this BCC metallic phase.

**Uranium-Zirconium Delta (C32) Phase**

The delta (δ) phase of Uranium-Zirconium is an important phase for non-high temperature conditions. The delta phase is observed during fuel fabrication and is the only intermetallic phase in the U–Zr system (Basak 2011).

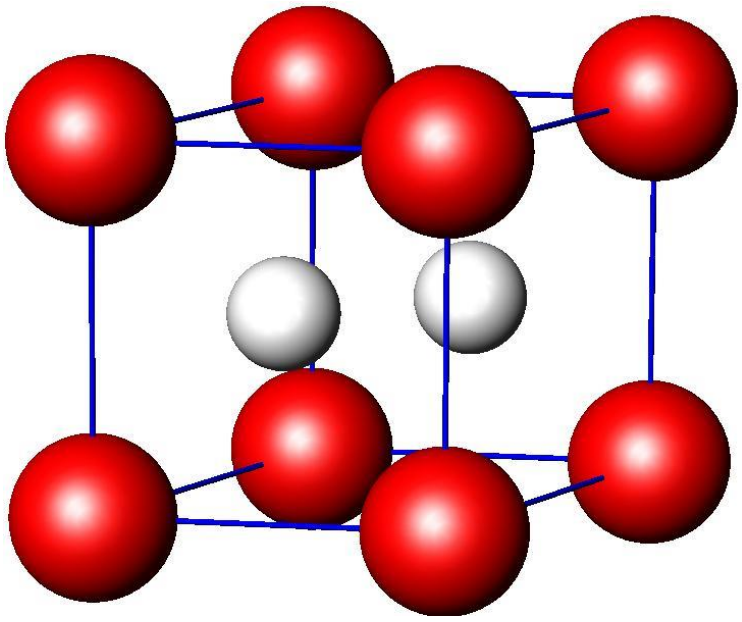

Figure 8: Unit Cell of the δ (C32) Ordered Phase U-Zr Crystal System ("Alb2 omega structure")

Table 1: Structure of the δ U-Zr Crystal System

| | |
|---|---|
| Pearson Symbol | hP3 |
| Space Group | P6/mmm |
| Prototype | Al-B2 |
| Strukturbericht Designation | C32 |

## Applications of Uranium-Zirconium

### Subcritical Advanced Burner Reactor (SABR)

The metallic fuels with their high heavy metal density and their complementary relationship with fast reactors allow engineers to consider new reactor designs. One of the new reactor designs that is being explored is the Subcritical Advanced Burner Reactor (SABR). The SABR design is unique because it uses a fusion neutron source (similar to ITER's tokamak) to drive the subcritical fast reactor. This design allows for large amounts of not highly enriched fuel to be burned. In addition, the subcritical nature of the reactor creates safety benefits (Stacey, unpublished data).

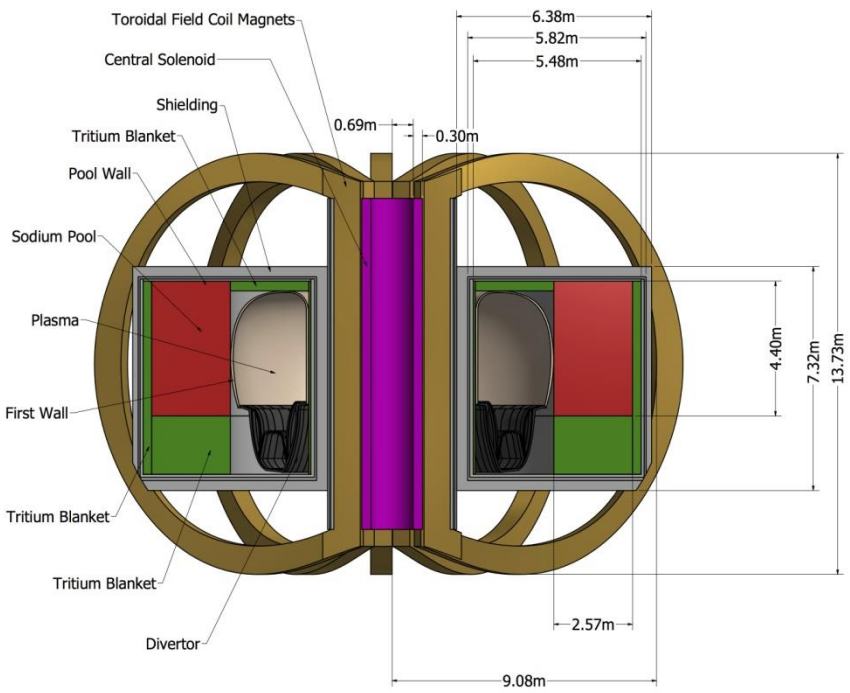


Figure 9: Perspective View of SABR Configuration. (Stacey, unpublished data)

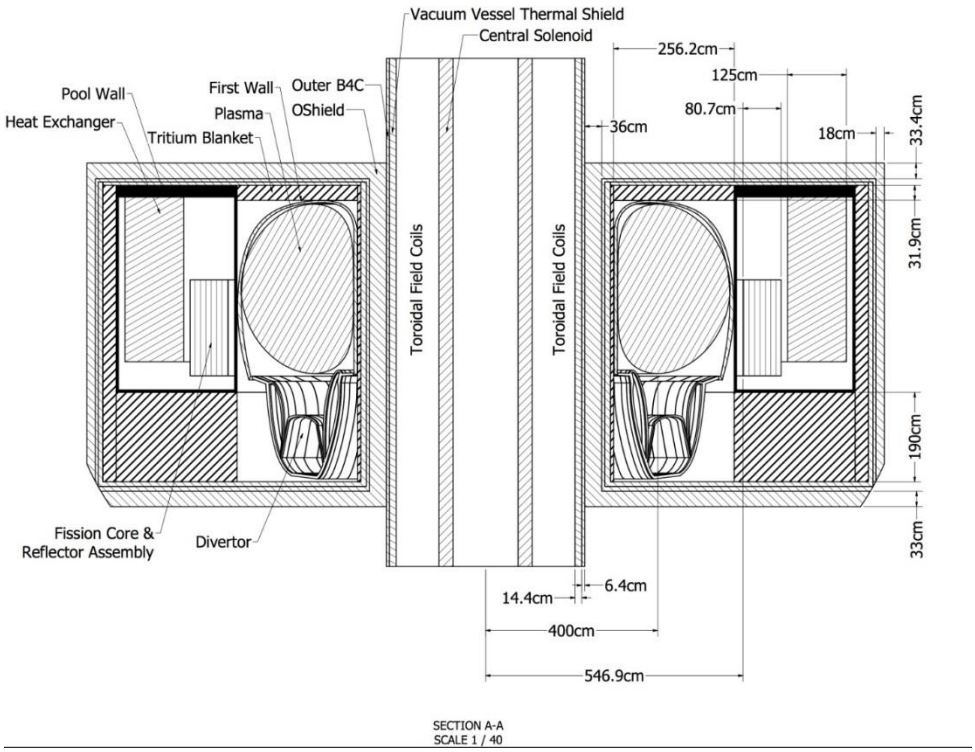


Figure 10: Radial Build of SABR Configuration (Stacey, unpublished data)

Table 2: Basic SABR Core Properties (Stacey, unpublished data)

| **Fast Reactor Core Properties** | |
|---|---|
| Coolant | Sodium (Na) |
| TRU fuel composition | 40Zr-10Am-10Np-40Pu |
| Fuel Maximum / Allowable Temperature | 1014 K / 1200 K |
| Cladding Maximum / Allowable Temperature | 814 K / 923 K |
| Coolant Maximum / Allowable Temperature | 787 K / 1156 K |
| BOL TRU mass | 15104 kg |
| BOL keff | 0.973 |
| Specific power | 198.6 W/gHM |
| Fuel assembly | 800 |
| Fuel pin | 469/per assembly, 375,200 total |

Table 2 Continued: Basic SABR Core Properties (Stacey, unpublished data)

| | |
|---|---|
| Power density | 256 kW/L |
| Linear fuel pin power | 12.3 kW/m |
| Sodium coolant mass flow rate | 16,690 kg/s |
| Coolant temperature Tincool/Toutcool | 628 K/769 K |
| Fuel & Clad temperature Tmaxfuel/Tmaxclad | 1014 K/ 814 K |
| Clad & Structure | ODS MA957 |
| Electric insulator | SiC |
| Fuel/Clad/Bond/Insulator/duct/coolant/wire (v/o) | 22.3/17.6/7.4/6.5/9.3/35.3/1.5% |

One of the problems this design had to overcome however was a significant amount of swelling and fission gas production that took place in the metallic fuel. Since SABR was designed for long fuel irradiation cycles with high burn-up the fission gas production was especially copious.

To overcome this obstacle, the fuel is fabricated with a 75% smear density and an extra-long plenum was introduced to hold the fission gasses that escaped the fuel. Normally swelling and fission gas production is an issue during operation with metallic fuels, but since the SABR design has very high burn-up conditions, it requires extra accommodations. The plenum was made to be almost twice as long as the fuel region, allowing the extra fission gas products to escape the fuel.

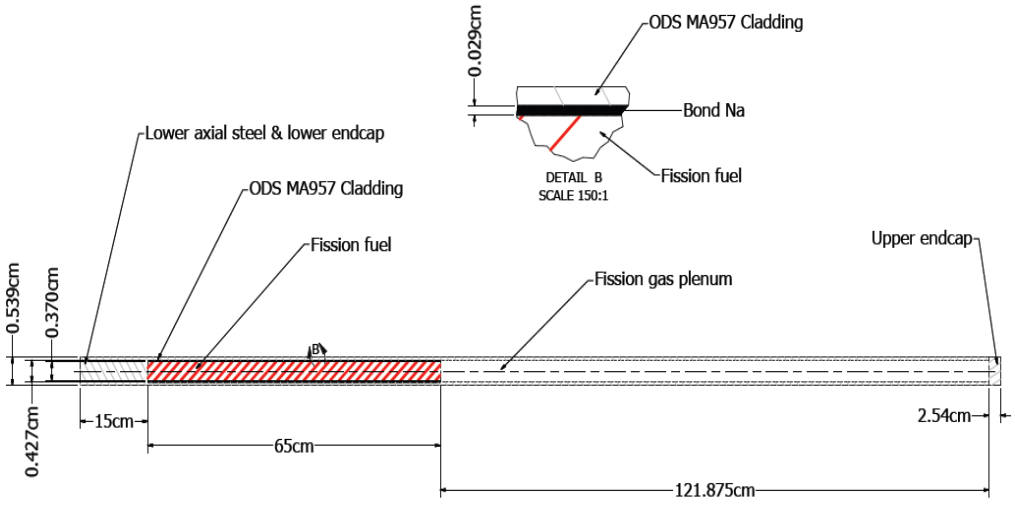


Figure 11: SABR Fuel Pin Configuration (Stacey, unpublished data)

Another problem the SABR design faces is the irradiation damage to the cladding. The cladding has an inherent irradiation limit that was experimentally determined before the irradiation damage causes changes in the cladding that could lead to cladding failure. The irradiation limit to the cladding coupled with the embrittlement and thinning of the cladding from Fuel Cladding Interactions (FCCI and FCMI), discussed in Metallic Fuel Disadvantages section, is another possible obstacle for the use of U-Zr. While, the SABR design keeps the cladding irradiation damage below the set limit, more research might be needed to incorporate the effect of Fuel Cladding interactions.

# CHAPTER 2

## COMPUTATIONAL THEORY & ANALYSIS

### Ensembles and Averaging

Computational methods allow for the analysis to explore the fundamental properties within materials. The detailed knowledge gained from computational simulations into the microstructural and atomistic properties of the fuels is required for the complete understanding of the macroscopic properties. The overall goal of these computational atomistic simulations is to understand and predict material responses to stimuli.

Macroscopic properties can be gleaned through an atomistic simulation. In an atomistic simulation a sequence of points, corresponding to atom positions, satisfying the conditions of a particular thermodynamic state are said to belong to the same ensemble. These sequences of atom positions describe the state of the system. An ensemble can be defined as a collection of all possible systems which have different microscopic states but have one or more identical macroscopic or thermodynamic extensive properties.

Ensembles are characterized by the independent variables, the variables that are held constant during simulation. Some variables need to be held constant to reduce the total number of variables in order to solve the system of classical motion equations and to be able to receive useful data corresponding to thermodynamics properties. During the course of atomistic simulations, including Molecular Statics (MS), Molecular Dynamics

(MD) and Metropolis Monte Carlo (MC), ensembles can be used to find the approximate equilibrium state for the dependent unfixed variables.

After the computational simulations have run for a while, it is commonly assumed that the dependent properties are fluctuating around the equilibrium value and an average can be constructed to approximate this equilibrium value.

$$\langle A \rangle = \sum_i A_i p_i \qquad (1)$$

This assumption of an ensemble average being the time average after initial fluctuations have died down is referred to as the Ergodic hypothesis for molecular dynamics (MD) simulations.

$$\langle A \rangle = \lim_{t \to \infty} \frac{1}{t} \int_0^t A \, dt \qquad (2)$$

Table 3: Common Thermodynamic Ensembles

| **Ensembles** | **Independent Variables** | **Dependent Variables** | **Z (Partition Function)** | **Pi (ith state Probability)** |
|---|---|---|---|---|
| Microcanonical | N, V, U | μ, P, T | $\sum_i \delta(E_i - E)$ | $\frac{\delta(E_i - E)}{Z_{NVE}}$ |
| Canonical | N, V, T | μ, P, E | $\sum_i e^{-\beta E_i(N,V)}$ | $\frac{e^{-\beta E_i(N,V)}}{Z_{NVT}}$ |
| Grand Canonical | V, T, μ | N, P, L | $\sum_i e^{\beta N \mu} Z_{NVT}$ | $\frac{e^{-\beta(E_i - \mu N)}}{Z_{NV\mu}}$ |
| Isothermal-Isobaric | N, P, T | μ, V, H | $\sum_i e^{\beta p V_i} Z_{NVT}$ | $\frac{e^{-\beta(E - pV_i)}}{Z_{NPT}}$ |

Where U is the total energy of the system, $\beta=1/k_BT$ is the reduced temperature, Z is the partition function, N is number of moles, V is volume, T is temperature, $\mu$ is the chemical potential, p is the pressure, H=U+PV is the enthalpy, $L=U-\Sigma(\mu_i N_i)$ is the Hill energy, $P_i$ represents the probability of observing the $i^{th}$ state and all of the other subscript i's represent the parameter at the $i^{th}$ state (Hünenberger 2005).

## Molecular Statics (MS)

Molecular static simulations (energy minimization) were performed using the "in-house" code DYNAMO (predecessor to LAMMPS or PARADYN). The process of an energy minimization simulation corresponds to relaxing (or moving) the atomic atoms positions until zero net force is acting on the system at 0K (Minimum Energy Configuration). Molecular Statics with DYNAMO uses the equations of motion from Newton's 2nd law to relax the atoms.

The force acting on an atom can be represented by the derivative of the potential energy over space.

$$F = -\frac{\partial U}{\partial r} \qquad (3)$$

The potential energy is obtained from using the interatomic potentials for all of the atoms in the system. The potential energy is often represented as a truncated taylor-series expansion as follows:

$$U(r+\delta r) = \mathrm{U}(r) + \frac{\partial U}{\partial r}\delta r + \frac{1}{2!}\frac{\partial^2 U}{\partial r^2}(\delta r)^2 + \cdots \quad (4)$$

The potential energy is truncated to the first derivative for each coordinate direction, called gradient vector (g), or sometimes to the second derivative in the coordinate systems, called a Hessian Matrix (H). DYNAMO uses the steepest descent method by taking the gradient vector of the potential energy for each atom resulting in forces acting on each atom in the system. Each atom is moved with a step size proportional to the force acting upon it. This procedure is repeated until an energy convergence criteria is met.

$$r_i^j = r_i^{j-1} + \alpha F_i \quad (5)$$

Where $r_i$ is the position of the $i^{th}$ atom, j is the iteration number, α is a multiplication factor, Fi is the force being exerted on the $i^{th}$ atom and α is the multiplication factor.

Since the BCC Uranium-Zirconium phase is unstable at 0K, energy minimization was performed by holding the atoms in the BCC phase and relaxing the unit cell.

## Molecular Dynamics (MD)

Molecular Dynamics (first principles) simulation consists of a numerical systematic solution to the classical equations of motion. Similarly to Molecular Statics, Molecular Dynamics calculates the force on each atom from the gradient vector of the potential energy at each atom's location. Molecular Dynamics computes the phase-space

trajectory, in which the atoms are allowed to interact for a period of time with forces being exerted on each atom, giving snapshots of the motion of atoms. The forces on each atom are calculated using the MEAM interatomic potential developed. Temperature in a Molecular Dynamics simulation corresponds to an average atom velocity.

The Molecular Dynamics code used, called DYANMO, was run under an Isothermal–isobaric (NPT) ensemble, in which the atoms, pressure and temperature are held constant. The initial simulation consists of a random solid solution of 2000 atoms with periodic boundary conditions in an un-relaxed, perfect BCC lattice.

**MD Time Convergence and Averaging**

The simulation must be run long enough to reach the equilibrium value and then additional time to ensure a good statistical average. The total MD simulation time was run for 100 picoseconds using a 2 femtosecond time step, with ensemble property averaging over the last 35 picoseconds. The root mean squared (RMS) value of the properties gives an idea of the variation or fluctuation of the properties during the simulation averaging time period.

**Equations of Motion**

Molecular dynamics simulation computes the phase space trajectory in response to forces. The three dimensional configuration of atoms in space is given by:

$$m_i \frac{d^2 \bar{r}_i}{dt^2} = F_i = -\frac{\partial U}{\partial \bar{r}_i} \qquad (6)$$

## Periodic Boundary Conditions (PBC) and Finite Size Effects

There are a variety of boundary conditions that can be used for computational simulation, but in order to represent the bulk mechanical properties, the simulations were performed using periodic boundary conditions in all dimensions.

Since the molecular dynamics (MD) simulation uses periodic boundary conditions, it is necessary to ensure that the system is sufficiently large enough to represent the system of interest accurately. Therefore, the potential energy from a random solid solution molecular dynamics (MD) simulation was analyzed for a range of sizes to determine an adequate size to minimize the periodic boundary finite size effects. However, larger systems have a dramatically longer computational runtime; therefore a balance is made to ensure size effects are negligible while keeping the computational runtime to a minimum.

Finite periodic box size effects are hard to quantify, especially for high temperatures where thermal scattering events can over dominate the finite periodic box effects. In addition, since a time average is taken of the properties, a larger box size will result in a better average due to the law of large numbers.

More drastically however, the box size can affect the overall MC-MD iteration configuration, not only does the box size have to be large enough to model the molecular dynamics accurately, but also it must allow for a size large enough for separation, clustering and ordering effects to be seen and have limited influence from the neighboring reflected images.

The cubic periodic box size was kept to 10x10x10 BCC unit cells, which together make a supercell, to minimize the periodic effects in the molecular dynamics simulation, where 10x10x10 is significantly larger than the minimum PBC size requirement of twice the cut-off radius distance ($r_{cut}$). This condition eliminates correlated fluctuations that atoms may experience due to simultaneous interactions with two images of a given particle.

The 10x10x10 BCC unit cells that form the supercell's cubic periodic boundary conditions (PBC) have problems replicating all of the equilibrium configuration effects seen in the MC-MD simulation. However, it will be able to replicate ordering trends and approximate the local minimum energy configuration needed for the enthalpy of mixing.

## Monte Carlo (MC)

The Monte Carlo (MC) simulation used is based on the Metropolis Monte Carlo algorithm (Metropolis 1953) (Wang 2005). The MC method allows for the study of order-disorder and segregation phenomena in the equilibrated system. The MC method is not based on the equations of motion, like the MD simulation, but the energetics of the states. This type of Monte Carlo simulation is good for evaluating effects that would take a long time to witness during a molecular dynamics simulation. In addition, this type of Mote Carlo simulation allows for insight into the possible range of thermodynamic properties which could change due to atomistic ordering effects.

Order-disorder transitions proceed through substitution between atoms followed by small atomic displacements. These order-disorder transitions are commonly found in metals and alloys. The Monte Carlo (MC) approach is used to drive the atoms toward their equilibrium state at a finite temperature.

The MC simulation started with the ending positions of each atom after the previous MD simulation. Then a series of configuration transformations were performed to achieve a thermo-dynamically equilibrated state. The Monte Carlo Code uses a canonical (or NVT) ensemble, which means that the number of atoms, volume, and temperature is conserved.

In each MC step, one of the following two configuration changes is attempted with an equal probability:

1. A randomly selected atom is displaced from its original position in a random direction with a distance between 0 and $r_{max}$, where $r_{max}$ is a function of temperature and is zero for 0 Kelvin.
2. Two randomly selected atoms with different elemental types are exchanged.

Operation (1) accounts for the positional relaxation processes (adjustment of bond lengths and angles), while operation (2) accounts for the compositional relaxation processes (segregation).

$$P_{XY} = \exp\left(\frac{-\Delta E}{k_B T}\right) \qquad (7)$$

After each configuration change, we evaluate the energy change between the new and old configurations. If $P_{XY} > 1$ (decrease in energy), the new configuration is accepted. If $P_{XY} < 1$ (increase in energy), the new configuration is retained with the probability $P_{XY}$. In the beginning of MC simulations, the potential energy of U–Zr decreases rapidly due to positional and compositional relaxations. However, when the simulations approach equilibrium, there is no significant change in potential energy and the acceptance rate of element exchange operations remains stable around a certain value (Wang 2005).

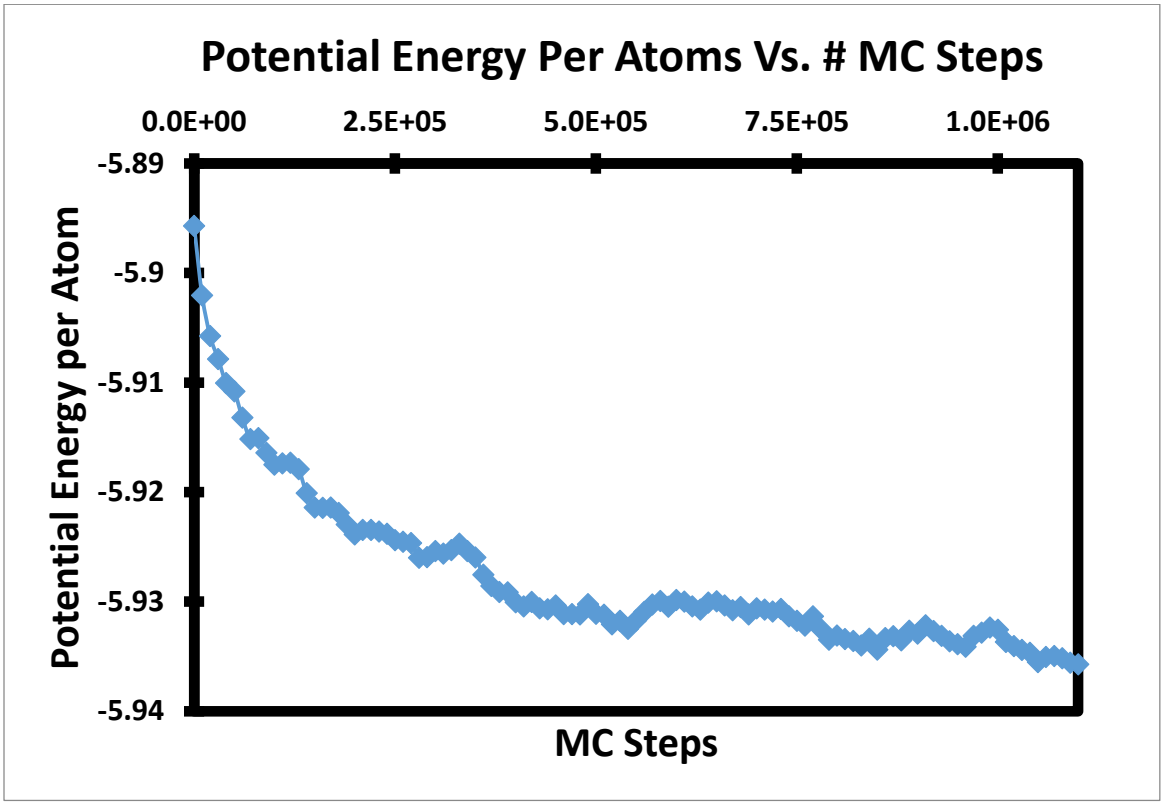


Figure 12: Number of MC-Steps U-Zr10 at a Temperature of 800 Kelvin

## Short Range Order (SRO) Parameter

Order parameters allow for the configurational and ordering changes to be represented by a value or a few values. Ordering parameters allow for the overall ordering trends to be easily seen.

The Short Range Order (SRO) parameter considers only first nearest neighbors (1NN). $P_{AA}$ is the fraction of the nearest neighbor sites of atom type A that are occupied by A type atoms (averaged over all A atoms). $n_A$ is the atomic fraction of A type atoms in the entire system.

$$\sigma = -\frac{P_{AA}-n_A}{1-n_A} \quad (8)$$

With this definition, $\sigma = 1$ for the perfectly ordered lattice, $\sigma = -1$ for the phase separated system, and $\sigma = 0$ for a random solid solution of equal numbers of A and B atoms. If the number of A and B atoms are unequal, the magnitudes of the extreme values of $\sigma$ are reduced.

**SRO: 1.0**

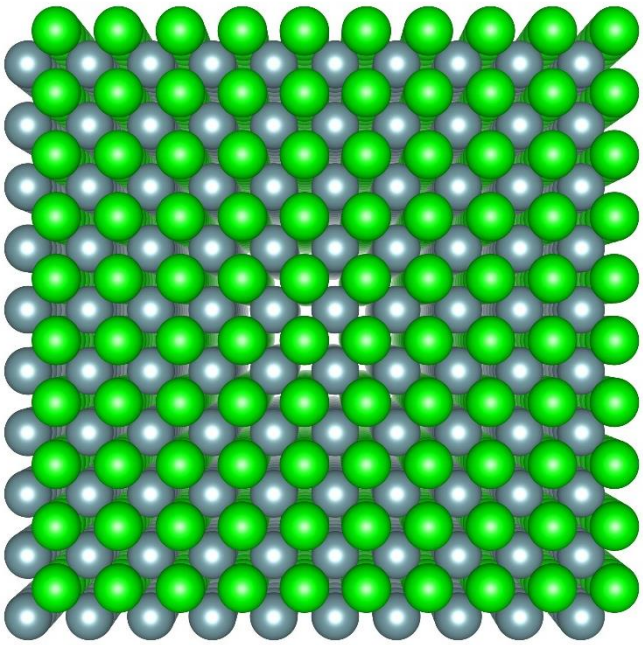

Figure 13: Perfectly Ordered Periodic B2 U-Zr System (Uranium 50% atomic fraction and Zirconium 50% atomic fraction)

**SRO: -0.8**

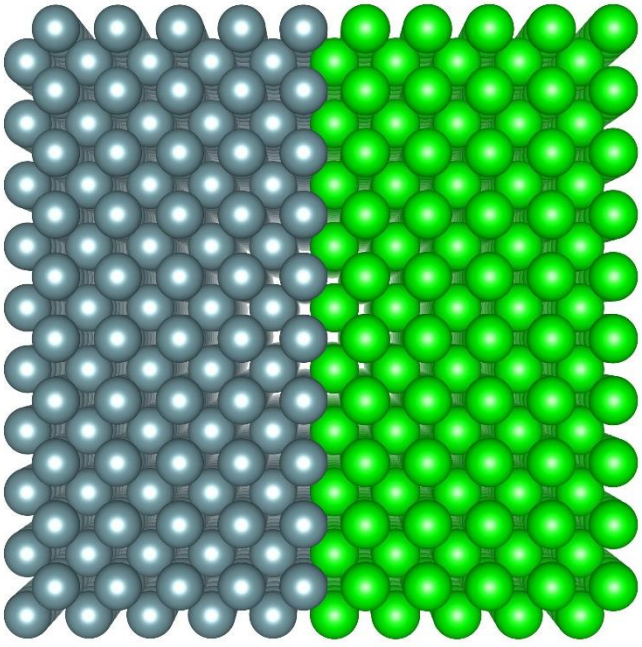

Figure 14: An Example of a Periodically Separated U-Zr System (Uranium 50% atomic fraction and Zirconium 50% atomic fraction)

For the separated case, we can never achieve the perfect separated short range order parameter of -1 since we have a finite box with periodic boundary conditions. The separated short range order parameter depends on both the finite periodic box size and the way the atoms separate, i.e. whether the atoms separate and are divided by a single planar line (seen in Figure 14 above) or bunch into a cluster of atoms.

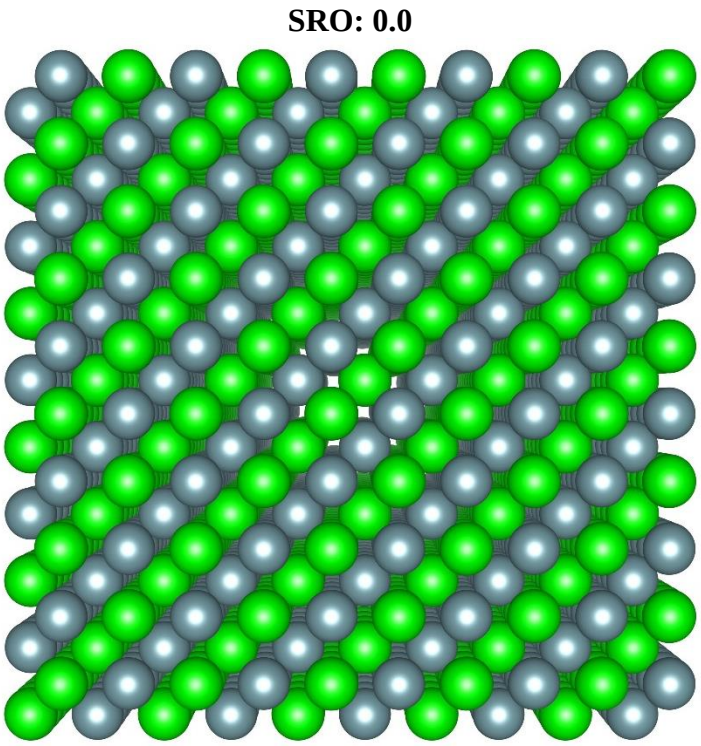


Figure 15: An Example of a Configuration of Planes of Atoms Not Captured by the Short Range Order Parameter

However, there are some configurations that are not able to be captured by the short range ordering parameter, and therefore visual verification is still performed. One of the structures that may form that cannot be captured by the SRO are alternating planes of atoms.

The Short Range Order parameter code assumes a Body Centered Cubic crystal structure and therefore eight nearest neighbor atoms. The order parameter is calculated on a snapshot of the atoms' positions at a given time.

### Molecular Statics/Dynamics (MS/MD) - Monte Carlo (MC) Iterations

The Monte Carlo (MC) simulation with an NVT ensemble rearranges the atoms to have a lower free energy. This restructuring of the atoms creates a problem since rearranging the atoms should cause a volume change. Running a Molecular Statics or a Molecular Dynamics simulation with an NPT ensemble corrects the volume problem. However, the corrected volume changes how the structure rearranges during an MC simulation. Therefore an iterative MC-MS and MC-MD simulation is proposed, which should eventually settle to the state that minimizes the free energy through a series of atom switching and thermal motion, if continued. This state may or may not be the lowest energy state since a series of simple atom switching will most likely result in a state which represents a local minimum instead of the global minimum of the free energy.

A finite number of MC-MS and MC-MD iterations is proposed to approximate the minimal free energy structure.

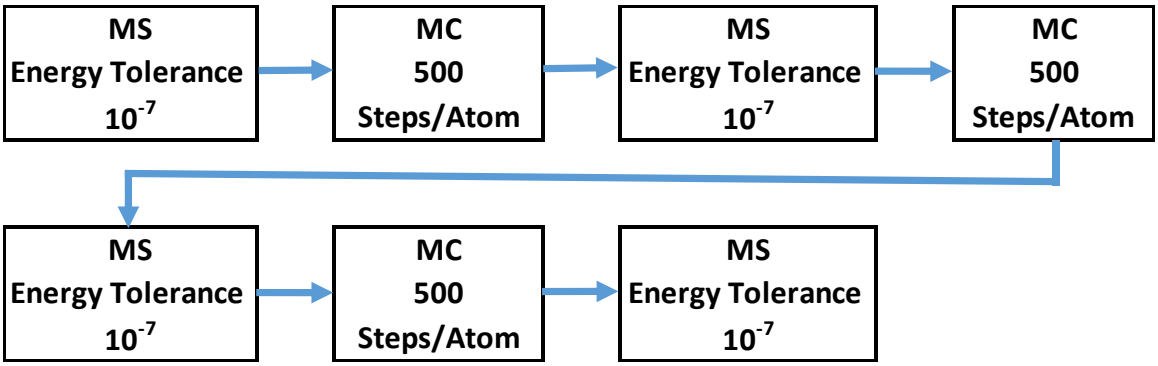


Figure 16: Flow Diagram of the Proposed Finite Iterative Molecular Statics (MS) and Monte Carlo (MC) Simulation

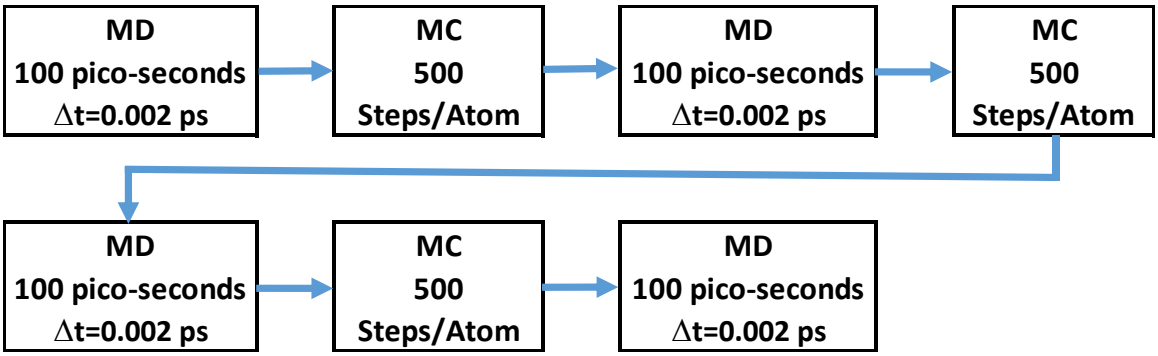


Figure 17: Flow Diagram of the Proposed Finite Iterative Molecular Dynamics (MD) and Monte Carlo (MC) Simulation (Moore 2013)

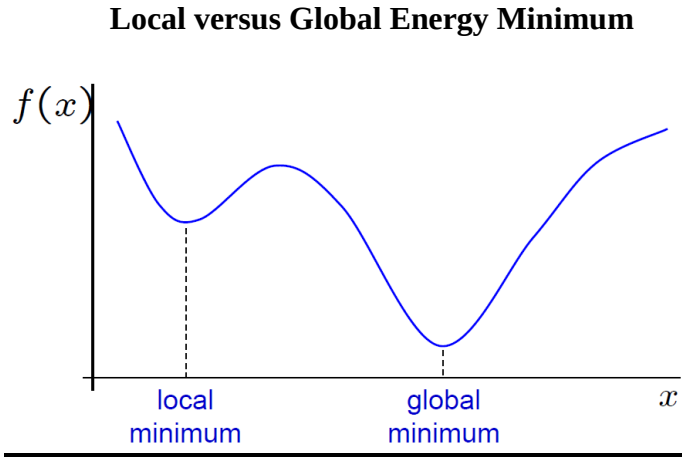


Figure 18: Graphical Representation of Local versus Global Minimum

Simulations searching for a minimum energy can become trapped in a local minimum energy region. While the overall energy minimum is the global minimum, the local minimum values still hold useful information.

This phenomenon has the most drastic effect on the Metropolis Monte Carlo Simulation. A finite number of simple atom switching most likely will not result in the global energy minimum but a local energy minimum configuration.

## Radial Distribution Function (RDF)

The radial distribution function (RDF) is a useful tool for atomic analysis of crystal systems. The radial distribution function gives a normalized equation of the distance between atoms in the lattice. The RDF is calculated by describing how the radial density from a reference particle varies as a function of radial distance from this reference particle. The RDF can be described by the function g(r), which gives the probability of finding a particle in the distance r from another particle.

$$\mathrm{g(r)} = \frac{1}{4\pi N r^2 \rho_0} \sum_{j=1}^{N} \sum_{\substack{i=1 \\ i \neq j}}^{N} \delta\left(r - r_{ij}\right) \qquad (9)$$

The calculation of g(r) can give useful information about the average thermal scatter (by looking at the width of the peaks) and the phase of the system (by looking at the distance between the peaks), and it can even give information on the chemical ordering in a complex system when elemental radial distance functions are used.

## Thermal Expansion

The volumetric thermal expansion for the body centered cubic (BCC) metal is assumed to be isotropic, which has been observed in experiments. The volumetric thermal expansion coefficient is described by the following equation:

$$\alpha_V = \frac{1}{V}\left(\frac{\delta V}{\delta T}\right)_p \quad (10)$$

where V is the volume, T is the temperature and the subscript p denotes a change under constant pressure. The coefficient of thermal expansion for the MEAM potential is obtained through molecular dynamics simulations with periodic boundary conditions in a NPT ensemble where the periodic volume is able to change at temperature changes.

While thermal expansion is experimentally measured on a multi-grain sample, we assume the grains and dislocations have a minimal effect on the overall value for thermal expansion. With this assumption we are able to compare the experimental values to the simulated bulk values.

## Atomistic Elastic Constants

For the elastic constants we use Hooke's law ($\sigma=E\varepsilon$). Hooke's law states that the stress is proportional to the gradient of the deformation occurring in the material. If a continuum material is a linear elastic material, we can introduce Hooke's law in Cartesian coordinates:

$$\sigma_{ij} = C_{ijkl}\varepsilon_{kl} \quad (11)$$

where $\sigma_{ij}$ is the stress, $\varepsilon_{kl}$ is strain and $C_{ijkl}$ are the elastic constants.

This equation assumes a linear relationship between the components of the stress tensor and strain tensor. In other words the Hooke's law gradient has been reduced to first and some second order differentials. In addition, since the simulation is of a bulk material, for the pure elemental simulations at 0K the material can be seen as homogenous, so that the elastic constants should be independent over the position in the crystal. Therefore we get the relation:

$$c_{ijkl} = c_{jikl} = c_{ijlk} = c_{jilk} \tag{12}$$

Consequently with this relationship, now only 36 of the 81 elastic constants are independent.

$$\begin{pmatrix} \sigma_1 \\ \sigma_2 \\ \sigma_3 \\ \sigma_4 \\ \sigma_5 \\ \sigma_6 \end{pmatrix} = \begin{pmatrix} c_{11} & c_{12} & c_{13} & c_{14} & c_{15} & c_{16} \\ c_{21} & c_{22} & c_{23} & c_{24} & c_{25} & c_{26} \\ c_{31} & c_{32} & c_{33} & c_{34} & c_{35} & c_{36} \\ c_{41} & c_{42} & c_{43} & c_{44} & c_{45} & c_{46} \\ c_{51} & c_{52} & c_{53} & c_{54} & c_{55} & c_{56} \\ c_{61} & c_{62} & c_{63} & c_{64} & c_{65} & c_{66} \end{pmatrix} \begin{pmatrix} \varepsilon_1 \\ \varepsilon_2 \\ \varepsilon_3 \\ \varepsilon_4 \\ \varepsilon_5 \\ \varepsilon_6 \end{pmatrix} \tag{13}$$

To reduce the elastic constants further, crystal symmetry can be introduced. Therefore, cubic crystal symmetries with four 3-fold rotational point symmetry can reduce the remaining 36 elastic constants to 3 elastic constants ($C_{11}$, $C_{12}$, and $C_{44}$) (Jaric 2008; Zener 1948). Similarly, a hexagonal crystal structure with one 6-fold rotational symmetry can reduce the 36 remaining elastic constants to 5 elastic constants ($C_{11}$, $C_{12}$, $C_{33}$, $C_{13}$, and $C_{44}$) (Li 1990; Tromans 2011). The reduction in elastic constants for cubic symmetry was shown by Zener (Zener 1948) and more recently by Jaric (Ledbetter 1973). While the reduction in elastic constants for hexagonal symmetry can be seen by Tromans (Tromans 2011).

The end cubic symmetry tensor Hooke's law results in the following:

$$\begin{pmatrix}\sigma_1\\ \sigma_2\\ \sigma_3\\ \sigma_4\\ \sigma_5\\ \sigma_6\end{pmatrix} = \begin{pmatrix}c_{11} & c_{12} & c_{12} & 0 & 0 & 0\\ c_{12} & c_{11} & c_{12} & 0 & 0 & 0\\ c_{12} & c_{12} & c_{11} & 0 & 0 & 0\\ 0 & 0 & 0 & c_{44} & 0 & 0\\ 0 & 0 & 0 & 0 & c_{44} & 0\\ 0 & 0 & 0 & 0 & 0 & c_{44}\end{pmatrix}\begin{pmatrix}\varepsilon_1\\ \varepsilon_2\\ \varepsilon_3\\ \varepsilon_4\\ \varepsilon_5\\ \varepsilon_6\end{pmatrix} \quad (14)$$

Another way to represent this Hooke's law matrix was created by Zener (Zener 1948), where he made relationships for cubic symmetries and defined two "Zener" elastic constants for cubic symmetries C and C'.

$$C = C_{44} \quad (15)$$

$$C' = \frac{(C_{11}-C_{12})}{2} \quad (16)$$

$$B = -\frac{\partial^2 U}{\partial V^2}V \cong \frac{C_{11}+2\,C_{12}}{3} \quad (17)$$

In the "Zener" notation, $C=C_{44}$ is the shear modulus, C' is the shear Zener constant, and B is the bulk modulus.

## Formation Energy

Formation energies were calculated starting by introducing defects into a supercell with equilibrium lattice constants and structural relaxation of atomic positions. When calculating defect formation energies, only non-interacting isolated defects were considered. In addition, in order to ensure that structural changes did not occur with the introduction of the defect, visual verification was used on the defect simulations.

The formation energy of a single vacancy in a homogenous bulk crystal that does not change phase can be described by:

$$E_v = E_{(n-1)} - \left[\frac{n-1}{n}\right] E_n \qquad (18)$$

where $E_{(n-1)}$ is the total energy of an (n-1) atom supercell containing one vacancy, and $E_n$ is the total energy of the structure with no vacancies.

Similarly, the formation energy of an interstitial can be defined as:

$$E_i = E_{(n+1)} - \left[\frac{n+1}{n}\right] E_n \qquad (19)$$

where $E_{(n+1)}$ is the total energy of an (n+1) atom supercell containing one interstitial, and $E_n$ is the total energy of the structure with no interstitials.

## Enthalpy of Mixing (Heat of Formation)

The enthalpy of mixing at zero Kelvin makes the temperature component of the free energy negligible; therefore, the change in the free energy comes from the change in the enthalpy of mixing. While physically the Body Centered Cubic Phase is unstable at zero Kelvin, to find the temperature effects of the MEAM potential on the enthalpy of mixing, the crystal structure was fixed to remain in the BCC configuration; Dr. Landa in his Monte Carlo and *ab-initio* simulations of Uranium-Zirconium (Landa 2009) used a similar methodology.

For exothermic solutions, $\Delta Hmix < 0$, the mixing of the solution results in a free energy decrease. However, the opposite is not necessarily true at all temperatures for endothermic solutions, $\Delta Hmix > 0$.

The enthalpy of a homogenous system is defined by

$$H = U + pV \quad (20)$$

where H is the enthalpy of the system, U is the internal energy, p is the pressure and V is the volume.

For inhomogeneous systems the enthalpy is the sum of the subsystems as shown by the following equation

$$H = \sum_i H_i \quad (21)$$

where i is the index of each subsystem. If there are continuously varying properties, the summation becomes an integral.

The enthalpy of mixing was calculated using the MEAM binary compound heat of formation for a non-ideal solution, similar to the methodology described by Jelinek in "Modified embedded atom method potential for Al, Si, Mg, Cu, and Fe alloys." (Jelinek 2012)

The enthalpy of mixing was obtained by using the basic definition of enthalpy and ensemble averages for Volume, Pressure, Potential Energy and Kinetic Energy. The pure Uranium and Zirconium ensemble average properties for a given temperature were taken and set to the component properties (e.g. $P_i$, $V_i$, and $U_i$). The alloy ensemble average

properties for a given concentration and temperature were taken and set to the "mixed" properties (e.g. $P_{mix}$, $V_{mix}$ and $U_{mix}$).

The mixed enthalpy of mixing values were separated by the random solid solution (MD simulation only) and the ordered solution (made by the MD-MC simulations). This method allows for a representative model of the MEAM potential on the enthalpy of mixing, given by the following equation:

$$\Delta H_{mix} = U_{mix} - \sum_i X_i U_i + P_{mix} V_{mix} + \sum_i X_i P_i V_i \quad (22)$$

The entropy of mixing for the binary alloy system is a more difficult problem to model, and will not be fully discussed in this thesis. However, for a simple approximation of the configurational mixing entropy of the system, a statistical mechanics methodology can be used for ideal materials:

$$\Delta S_{mix} = -R[X_U \ln(X_U) + X_{Zr} \ln(X_{Zr})] \quad (23)$$

Once the enthalpy of mixing, temperature and the entropy of mixing are known, the Gibbs free energy of mixing can be found using the following equation:

$$\Delta G_{mix} = \Delta H_{mix} - T\Delta S_{mix} \quad (24)$$

# CHAPTER 3

## INTERATOMIC POTENTIAL

Density Functional Theory (DFT) states that energy is a functional of the electron density. Therefore, if the electron density is known everywhere in the system, the potential energy can be determined from that information using the following equation:

$$U = f[\rho(R)] \quad (25)$$

$$E[\rho(r)] = T_s[\rho(r)] + J[\rho(r)] + E_{xc}[\rho(r)] + E_{ext}[\rho(r)] + E_{ii}[r] \quad (26)$$

where E is the total energy, $T_s$ is the single particle kinetic energy, J is the Hartree-Electron-Electron Energy, $E_{xc}$ is the Exchange Correlation Functional, $E_{ext}$ is the Electron-Ion Coulombic interaction and $E_{ii}$ is the Ion-Ion energy.

The electron density is the underlying principal quantity for the Density Functional Theory (DFT). The electron density can be defined by the probability of an electron being present at a specific location. In mathematical terms it can be described as the integral of the wave function $\psi$ over the spin coordinates of all electrons over all but one of the spatial variables ($\vec{x} \equiv \vec{r}, s$), and is given by the following equation:

$$\rho(\vec{r}) = N \int \dots \int |\psi(\vec{x}_1, \vec{x}_2, \dots, \vec{x}_N)|^2 d\vec{x}_1 d\vec{x}_2 \dots d\vec{x}_N \quad (27)$$

where $\rho(\vec{r})$ is the probablilty of finding any of the N electrons within the volume element $d\vec{r}$. (Hohenberg 1964; Kohn 1965)

The electron density functional theory's concept of electron density's replacement of wave functionals led to the creation of the Embedded Atom Method (EAM) potential. The EAM potential is based on the assumption that an atom can be embedded into a homogenous electron gas, and that the resulting change in potential energy is a functional of the embedded atom electron density that can be approximated with an embedding function.

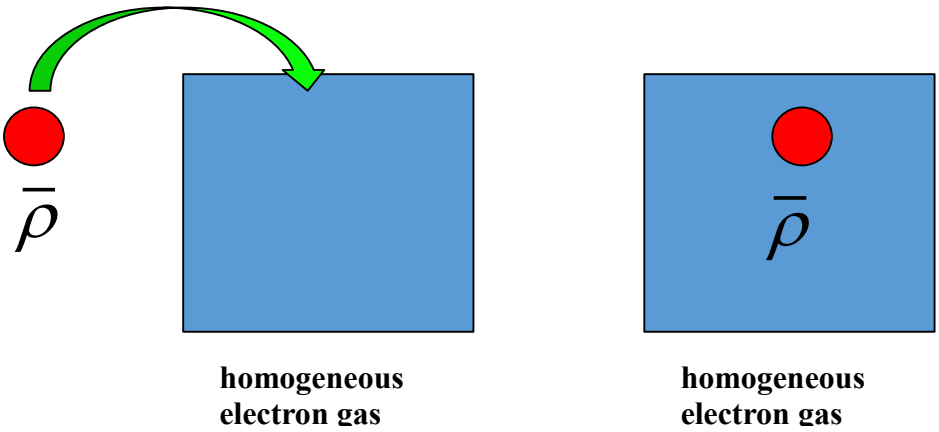


Figure 19: Physical Representation of the Basics of the Embedding Function (Baskes, unpublished data)

However, the electron density in a crystal is not homogenous. Therefore the EAM potential changes the background electron density to the electron densities for each atom and supplements the embedding energy by a repulsive pair potential to represent atoms core-core interactions.

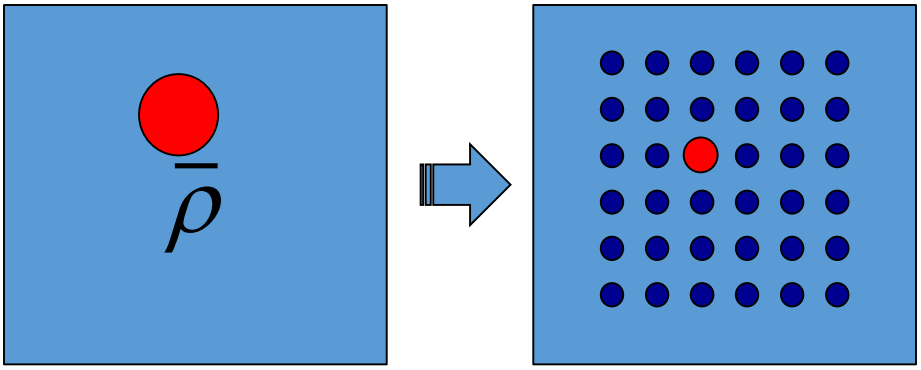


Figure 20: Physical Representation of the Embedding Function into a Lattice (Baskes, unpublished data)

The EAM potential uses a simple linear superposition of the atoms' electron densities as the background electron density.

$$\bar{\rho}_i = \sum_j \rho_j^a(R_{ij}) \quad (28)$$

$$R_{ij} = |r_i - r_j| \quad (29)$$

In the equations above, $R_{ij}$ is the distance between atoms i and j, $\rho_j^a$ is the atomic electron density and $r_i$ is the position of atom i.

The Embedded Atom Method (EAM) potential is a semi-empirical potential developed by Daw and Baskes in 1983 and has been used to successfully model a variety of face centered cubic (FCC) metals. The EAM inter-atomic potential does not simply depend on atom locations, but includes many body effects that depend on the local environment.

The potential energy of a crystal system, using the EAM potential, can be calculated using the embedding function F, the electron densities $\rho_i$ and the pair interaction potential $\phi$.

$$U = \sum_i F(\bar{\rho}_i) + \frac{1}{2}\sum_{i,j} \phi\left(R_{ij}\right) \quad (30)$$

## MEAM

However, the EAM potential has problems simulating materials with significant directional bonding, and cannot be used when simulating these materials. Criteria for significant directional bonding in materials were created using the Cauchy Relation or Cauchy Discrepancy which relates the $c_{12}$ and the $c_{44}$ elastic moduli for symmetrically cubic materials. The Cauchy Relation stated that the transverse expansion elastic constant ($c_{12}$) is equal to the shear modulus elastic constant ($c_{44}$) or $C_{12}=C_{44}$ (Born and Huang 1954) if the crystal and the atoms have cubic symmetry. This condition is not satisfied for most metals. Therefore materials with $C_{12}/C_{44} - 1 < 0$ (Cauchy Discrepancy) are said to have a significant amount of directional bonding and cannot be described by EAM (Born 1954).

The Modified Embedded Atom Method (MEAM) potential builds off the EAM potential by allowing the background electron density to depend on the local environment whereas the EAM potential uses a linear superposition of spherically averaged electron densities.

The MEAM inter-atomic potential is a semi-empirical potential proposed by Baskes et al. (Baskes 1992) that has been successfully used to reproduce the physical properties of various metals with different crystal structures. The MEAM potential is useful because it has the ability to replicate physical properties while keeping the computational power and time, which are necessary to complete the simulations, down to an acceptable level. This is a large step in making a fuel performance code and an accurate irradiation damage code.

The MEAM potential for a single element contains 14 adjustable parameters used to obtain the physical properties seen by experiments or *ab-initio* simulations. However, the MEAM potential becomes more complex for binary and tertiary alloys. A binary alloy has 14 adjustable parameters for each element and at least 15 adjustable parameters for the binary alloy interactions.

A MEAM potential is presented for the high temperature body-centered cubic (gamma) phase of U. MEAM potentials add an angular component to the older EAM potential to account for directional bonding.

With the MEAM potential, the total energy E of a system of atoms is given by:

$$U = \sum_i F(\bar{\rho}_i) + \frac{1}{2}\sum_{i,j\neq i} \phi_{ij}(R_{ij})\, S(R_{ij}) \qquad (31)$$

where $F_i$ is the embedding function, $\rho_i$ is the background electron density at site I, S is the radial screening and $\varphi_{ij}(R_{ij})$ is the pair interaction between atoms i and j at a distance $R_{ij}$.

**Embedding Function**

The embedding function describes the energy it takes to add (or embed) the atom to the crystal structure. The embedding function for the MEAM potential is defined by:

$$F_i(\bar{\rho}_i) = A_i E_{ci} \left(\frac{\bar{\rho}_i}{\rho_i^e}\right) ln \left(\frac{\bar{\rho}_i}{\rho_i^e}\right) \quad (32)$$

where A is an adjustable parameter, Ec is the cohesive energy, and $\rho^e$ is the electron density evaluated at equilibrium in the reference structure.

**Universal Binding Energy Relationship (UBER)**

The reference state energies are found from the Universal Binding Energy Relationship (UBER), which uses a reference structure to help create the pair potential. The UBER describes cohesion and adhesion of unrelaxed surfaces, chemisorption and diatomic molecules (Rose 1983). The UBER in the MEAM is normally fit through a few parameters.

The pair potential, instead of being given explicitly, is given as a functional of an embedding atom function and a universal function ($E^u(R)$) that is able to reproduce the universal equations of state (EOS) (Rose 1984) for the potential energy of a reference crystal structure. The universal function ($E^u(R)$) describes the uniform expansion or contraction in the reference structure.

The value of the energy per atom for the equilibrium reference structure is obtained from the zero-temperature universal equation of state by Rose et al.(Rose 1984) as a function of nearest-neighbor distance R:

$$E^u(R_{ij}) = -E_c\left[1 + a^* + \delta(a^*)^3\frac{r_e}{R_{ij}}\right]e^{-a^*} \quad (33)$$

$$a^* = \alpha(R_{ij}/r_e - 1) \quad (34)$$

$$\alpha = (9B\Omega/E_c)^{1/2} \quad (35)$$

The repulse and attract parameters of the MEAM potential are the short range attraction and repulsion forces in the UES (the cubic repulsion/attraction term in the Rose Energy).

**Reference State & Pair Potential**

The universal equation of state (EOS) combined with a reference structure can be back-calculated to a pair potential.

For the reference state:

$$E^u(R_{ij}) = F\left[\overline{\rho^0}(R_{ij})\right] + \frac{1}{2}\sum_{i,j}\phi(R_{ij}) = -E_c\left[1 + a^* + \delta(a^*)^3\frac{r_e}{R_{ij}}\right]e^{-a^*} \quad (36)$$

The equation can be re-written in the first nearest neighbor MEAM form of:

$$E^u(R_{ij}) = F\left[\overline{\rho^0}(R_{ij})\right] + \left(\frac{Z_1}{2}\right)\phi(R_{ij}) \quad (37)$$

where $Z_1$ is the number of first nearest neighbor atoms. The equation can be rearranged to get the pair potential as follows:

$$\phi(R_{ij}) = \left(\frac{2}{Z_1}\right)\left\{E^u(R_{ij}) - F\left[\overline{\rho^0}(R_{ij})\right]\right\} \quad (38)$$

where $\bar{\rho}^0$ is the background electron density for the reference structure.

**Background Electron Density**

The background density depends on the local environment, in particular the atoms' angular relation to one another. These angular contributions are split into partial electron densities. The background electron density ($\bar{\rho}$) is composed of a spherically symmetrical partial electron density $\bar{\rho}_i^{(0)}$ and angular partial electron densities $\bar{\rho}_i^{(1)}$, $\bar{\rho}_i^{(2)}$ and $\bar{\rho}_i^{(3)}$, and has the following form:

$$\left(\rho_i^{(0)}\right)^2 = \left[\sum_{j\neq i}\rho_j^{a(0)}(R_{ij})\right]^2 \quad (39)$$

$$\left(\rho_i^{(1)}\right)^2 = \sum_\alpha\left[\sum_{j\neq i}\frac{R_{ij}^\alpha}{R_{ij}}\rho_j^{a(1)}(R_{ij})\right]^2 \quad (40)$$

$$\left(\rho_i^{(2)}\right)^2 = \sum_{\alpha,\beta}\left[\sum_{j\neq i}\frac{R_{ij}^\alpha R_{ij}^\beta}{R_{ij}^2}\rho_j^{a(2)}(R_{ij})\right]^2 - \frac{1}{3}\left[\sum_{j\neq i}\rho_j^{a(2)}(R_{ij})\right]^2 \quad (41)$$

$$\left(\rho_i^{(3)}\right)^2 = \sum_{\alpha,\beta,\gamma}\left[\sum_{j\neq i}\frac{R_{ij}^\alpha R_{ij}^\beta R_{ij}^\gamma}{R_{ij}^3}\rho_j^{a(3)}(R_{ij})\right]^2 - \frac{3}{5}\sum_\alpha\left[\sum_{j\neq i}\frac{R_{ij}^\alpha}{R_{ij}}\rho_j^{a(3)}(R_{ij})\right]^2 \quad (42)$$

In these equations, $\rho_j^{a(h)}$ are the atomic electron densities of atom j at the distance $R_{ij}$ relative to the site i.

The atomic electron densities are given by:

$$\rho_j^{a(h)}(R_{ij}) = \rho_0 \, S_{ij} \, f_{cut}(R_{ij}) \, exp\left[-\beta^{(h)}\left(\frac{R_{ij}}{r_e} - 1\right)\right] \qquad (43)$$

where $\beta^{(h)}$ is the partial electron density decay, $r_e$ is the nearest neighbor distance, $S_{ij}$ is the screening factor, $f_{cut}$ is the cut-off function, and $\rho_0$ is a scaling factor which plays no role for pure elements, but has a significant role for alloy systems.

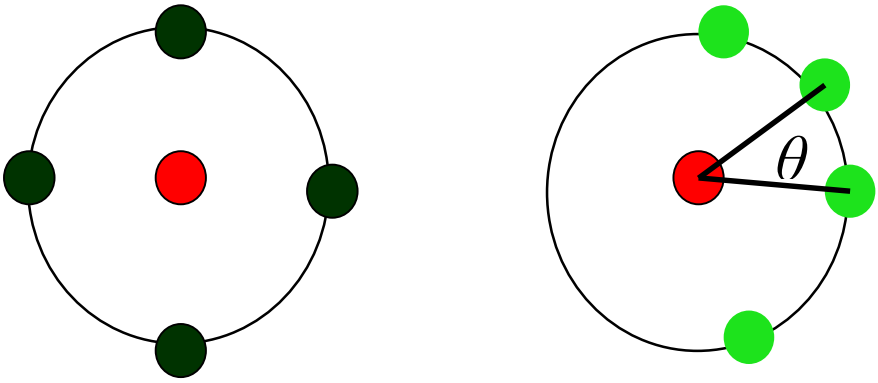


Figure 21: Physical Interpretation of directional bonding by partial electron densities (Baskes, unpublished data)

The geometric way $\rho_i^{(l)}$ is defined allows us to consider the partial background electron densities relate to the specific angular momentum contributions to the background electron densities known as electron orbitals(spdf). The partial background electron densities are orthogonal and can also be written in terms of Legendre polynomials.

$$\left(\rho_i^{(l)}\right)^2 = \sum_{j\neq i}\sum_{k\neq i}\rho_j^{a(l)}(R_{ij})\rho_k^{a(l)}(R_{ik})P_l^0\left(cos\left(\theta_{ikj}\right)\right) \quad (44)$$

$P_l^0$ are the Legendre polynomials:

$$P_0^0(z) = 1 \quad (45)$$

$$P_1^0(z) = z \quad (46)$$

$$P_2^0(z) = z^2 - \frac{1}{3} \quad (47)$$

$$P_3^0(z) = z^3 - \frac{3}{5}z \quad (48)$$

The total background electron density can be obtained from the weighted partial background electron densities through an intermediate term Γ:

$$\bar{\rho}_i = \rho_i^{(0)}\sqrt{1+\Gamma} \quad (49)$$

$$\Gamma = \sum_{l=0}^{3} t_i^{(l)}\left(\frac{\rho_i^{(l)}}{\rho_i^{(0)}}\right)^2 \quad (50)$$

where $t_i^{(l)}$ can be seen as the weighting factor for each of the partial electron densities. For convenience $t^{(0)} = 1$. Setting one value helps to visualize changes in the weighted parameters since the electron density is weighted by the t parameters.

**Screening**

Screening between two atoms (I and j) is defined as the product of screening factors, $S_{ijk}$, due to the neighboring atoms (k) that contribute to screening.

$$S_{ij} = \prod_{k \neq i,j} S_{ijk} \quad (51)$$

Consider a two-dimensional model of screening, leading to an ellipse method of describing screening. If the atoms i and j lie on the x-axis and the atom k is somewhere in the x,y plane that does not lie on top of either atom, an ellipse model can be used to describe the regions of screening.

Atom screening can be visualized using the ellipse model seen in Figure 22. In this model, atoms i and j are being screened by atom k. The amount of screening is separated into 3 regions: completely screened, partially screened, and non-screened.

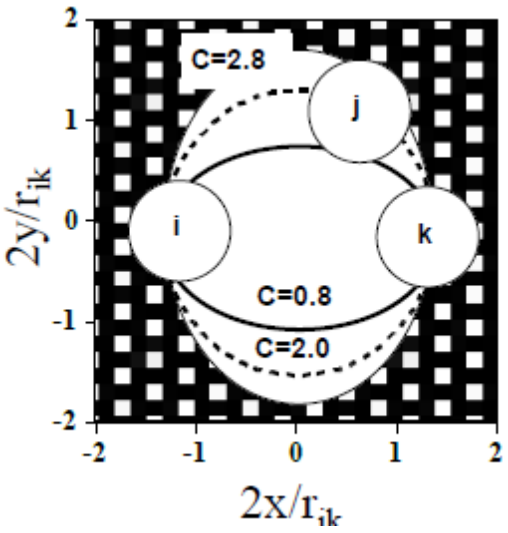


Figure 22: Visual Representation of MEAM Screening with an Ellipse (Baskes, unpublished data)

From this two-dimensional interpretation of screening, an equation can be made to represent the ellipse:

$$x^2 + \left(\frac{1}{C}\right) y^2 = \left(\tfrac{1}{2} R_{ij}\right)^2 \quad (52)$$

The ellipse parameter C is determined by a function of ratios between atoms i,j and k given by:

$$C = \frac{2(X_{ik}+X_{kj})-(X_{ik}-X_{kj})^2-1}{1-(X_{ik}-X_{kj})^2} \quad (53)$$

where: $X_{ik} = \left(R_{ik}/R_{ij}\right)^2$ and $X_{kj} = \left(R_{kj}/R_{ij}\right)^2$. The screening factor Sikj is defined as:

$$S_{ikj} = f_c[(C - C_{min})/(C_{max} - C_{min})] \quad (54)$$

where Cmin and Cmax determine the extent of the screening and fc is the cut-off function.

**Cut-Off Function**

The cutoff function describes the smooth, gradually decreasing distance effect on the interactions between the atoms. The smooth cut-off screening function (fc) is defined:

$$f_c(x) = 1, \quad x \geq 1$$
$$[1 - (1 - x)^6]^2, \quad 0 < x < 1,$$
$$0, \quad x \leq 0 \quad (55)$$

$$x = \left( \frac{R_{ij}^{cut-off} - R_{ij}}{\Delta R_{ij}} \right) \quad (56)$$

where Δ is the width of the cut-off region and $R^{cut\text{-}off}$ is the maximum cut-off distance. Normally, MEAM cut-off function has the (1-x) term to the fourth power rather than the sixth. However, the power was changed to the sixth when fitting the stacking fault energy for zirconium.

## 2nd Nearest Neighbor (2NN) MEAM

The main difference between the 1NN MEAM and the 2NN MEAM is that the 2NN MEAM attempts to incorporate 2NN atomic interactions, which are weaker than 1NN interactions, into the pair interaction term ϕ. The 1NN MEAM is able to neglect the second nearest neighbor interactions through the use of a strong many-body screening function. However, the 2NN MEAM is able to include second nearest neighbor interactions by adjusting the many-body screening function so that it becomes less severe.

Screening can play a large role on many parameters as temperature changes. Thermal vibration can cause atoms to drift in and out of various screening regions. When implementing the1st Nearest Neighbor (NN) MEAM, the screening parameters are selected to ensure that the first nearest neighbors are entirely un-screened. This "strong" screening allowed for the neglect of 2NN interactions, with only 1NN interactions being considered. The strong screening was taken into account by the many body screening function from a large minimum initial screening distance (Cmin).

However, for 2nd NN MEAM potentials the start initial minimum distance that screening starts (Cmin) is reduced, leading to a screening function that is less "strong" and incorporates second nearest-neighbor interactions. The UBER relationship for 2NN MEAM is slightly different due to the fact that the second nearest neighbor energy contributions have to be added.

$$E^u(R_{ij}) = F\left[\overline{\rho^0}(R_{ij})\right] + \frac{1}{2}\sum_{i,j}\phi(R_{ij}) \quad (57)$$

$$E^u(R_{ij}) = F\left[\overline{\rho^0}(R_{ij})\right] + \left(\frac{Z_1}{2}\right)\phi(R_{ij}) + \left(\frac{Z_2 S}{2}\right)\phi(aR_{ij}) \quad (58)$$

$$E^u(R_{ij}) = -E_c\left[1 + a^* + \delta(a^*)^3\frac{r_e}{R_{ij}}\right]e^{-a^*} \quad (59)$$

$$a^* = \alpha\left(R_{ij}/r_e - 1\right) \quad (60)$$

$$\alpha = (9B\Omega/E_c)^{1/2} \quad (61)$$

Here, $Z_2$ is the number of 2nd NN atoms, a is the ratio between the second and first nearest-neighbor distances, and S is the screening function on the second nearest-neighbor interactions. It should be noted that the screening function S is a constant for a given reference structure, if a value is given to Cmax and Cmin.

By introducing another pair potential, ψ(R), the equation above can be written as:

$$E^u(R_{ij}) = F\left[\overline{\rho^0}(R_{ij})\right] + \left(\frac{Z_1}{2}\right)\psi(R_{ij}) \quad (62)$$

$$\psi(R_{ij}) = \phi(R_{ij}) + \left(\frac{Z_2 S}{Z_1}\right)\phi(aR_{ij}) \quad (63)$$

Now, ψ(R) can be calculated from the equation as a function of R. Then, the pair potential ϕ(R) is calculated using the following relation:

$$\phi(R_{ij}) = \psi(R_{ij}) + \sum_{n=1}(-1)^n \left(\frac{Z_2 S}{Z_1}\right)^n \psi(a^n R_{ij}) \quad (64)$$

Here, the summation is performed until the correct value of energy is obtained for the equilibrium reference structure (Lee 2001).

**2NN Alloy MEAM**

To describe an alloy system, the pair interaction between different elements should be determined. In the 2NN MEAM, a perfectly ordered binary intermetallic compound, where only one type of atom has different atoms as first nearest-neighbors, is considered to be a good reference structure for creating the alloy pair potential. The B1 (NaCl type) reference structure is used for the U-Zr MEAM potential. For the B1 reference structure, the total energy per atoms (for half i atoms and half j atoms), $E_{ij}^u(R)$, is given by:

$$E_{ij}^u(R) = \frac{1}{2}\left\{F_i(\bar{\rho}_i) + F_j(\bar{\rho}_j) + Z^{ij}\phi_{ij}(R) + \frac{1}{2}Z_2^{ij}\left(\phi_{ii}(aR) + \phi_{jj}(aR)\right)\right\} \quad (65)$$

where $Z^{ij}$ is the number of second nearest-neighbor atoms in the reference structure. $\phi_{ii}$ and $\phi_{jj}$ are pair interactions between i atoms and between j atoms, respectively, and a is the ratio between the second and first nearest-neighbor distances. The procedure of

computing $\rho_i$ and $\rho_j$ is not different from that in 1NN MEAM except that the contribution from the second nearest-neighbors should also be considered. The pair interactions between the same types of atoms can be computed from the descriptions of individual elements (Lee 2001).

$$\phi_{ij}(R) = \frac{1}{Z_{ij}}\left\{2E_{ij}^{u}(R) - F_i(\bar{\rho}_i) - F_j(\bar{\rho}_j) - \frac{1}{2}Z_2^{ij}\left(\phi_{ii}(aR) + \phi_{jj}(aR)\right)\right\} \quad (66)$$

The cohesive energy for the alloy is determined by the elemental cohesive energies and a formation parameter $\Delta_{ij}$.

$$E_{ij}^{0} = \frac{\left(E_i^0 + E_j^0\right)}{2} - \Delta_{ij} \quad (67)$$

**MEAM U-Zr Alloy Reference Structure**

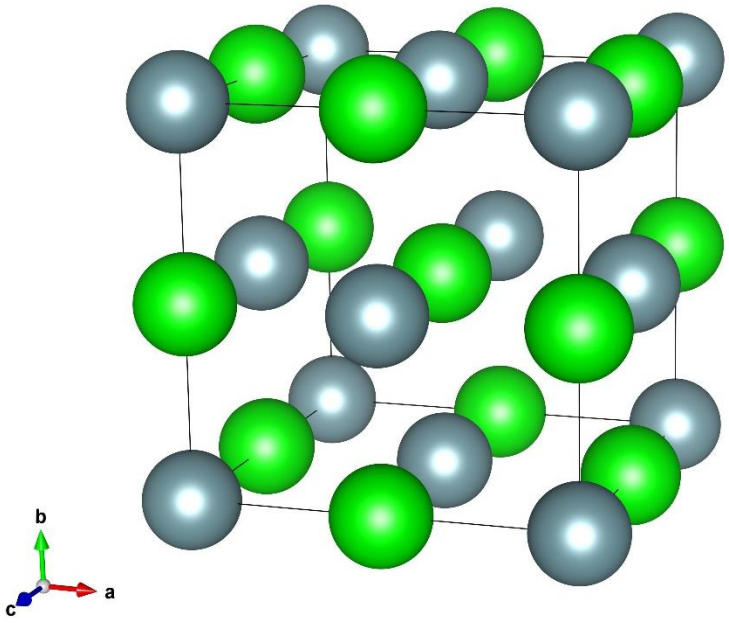


Figure 23: Unit Cell of the B1 U-Zr Reference Crystal Structure

Table 4: Structure Details of the B1 U-Zr Reference Crystal Structure

| | |
|---|---|
| Pearson Symbol | cF8 |
| Space Group | Fm3m |
| Prototype | Na-Cl |
| Strukturbericht Designation | B1 |

# CHAPTER 4

## RESULTS & DISCUSSION

### Uranium-Zirconium (U-Zr) 2NN MEAM Potential

Uranium had not been modeled with interatomic potentials until 2012, when three different papers came out in the same year (Beeler 2012b)(Smirnova 2012)(Yangzhong Li 2012). Elemental MEAM potentials for Uranium and Zirconium as well as alloy and screening parameters are need to be defined. For the pure Uranium MEAM potential used is built off the Uranium potential developed by Dr. Beeler (Beeler 2012b). While a few Zirconium MEAM potentials already existed, none were built primarily for the high temperature βZr phase. Therefore a new Zirconium MEAM potential had to be formulated as well as the alloy parameters.

The MEAM potentials for Uranium (Beeler 2012b) and Zirconium (Kim 2006; Bauer 1959) have been adjusted for use in the U-Zr alloy. This potential is the first interatomic U-Zr potential that has been made. It is important for the MEAM potential of the U-Zr binary alloy to capture some of the physical properties including the crystal structure, thermal expansion, enthalpy of mixing, and phase transitions.

The high percentage of Uranium is not analyzed for this MEAM potential, and some of the more complex phases will also not be analyzed, as they play lesser roles in the physical properties for the temperature range in question.

## Elemental MEAM Parameters

The parameters for the 2nd Nearest Neighbor MEAM potential are:

Table 5: Uranium Elemental Modified Embedded Atom Method (MEAM) Potential Parameters (Beeler 2012b)

| Elemental Uranium MEAM Parameters | Value | Description of Parameter or Source when Fitting |
|---|---|---|
| lat | FCC | Reference Lattice |
| Ec | 5.27 | Cohesive Energy of α/γ/fcc |
| α | 5.1 | Bulk modulus of γ |
| A | 1.04 | Relative stability of α and γ |
| $\beta^{(0)}$ | 6 | Relative stability of fcc and γ |
| $\beta^{(1)}$ | 6.8 | Shear elastic constants of α |
| $\beta^{(2)}$ | 7 | Shear elastic constants of α and γ |
| $\beta^{(3)}$ | 7 | Shear elastic constants of γ |
| $t^{(0)}$ | 1 | Set to allow as reference |
| $t^{(1)}$ | 2.5 | Vacancy formation energy in γ |
| $t^{(2)}$ | 4 | Shear elastic constants of α and γ |
| $t^{(3)}$ | 3 | Atomic volume of α |
| alat | 4.36 | Lattice constant of γ |
| $\rho^0$ | 1 | Background Electron Density Scaling |
| δ (attract=repulse) | 0.1 | Thermal expansion of γ |
| $C_{min}$ | 1 | Cohesive energy of α/γ/fcc |
| $C_{max}$ | 1.9 | Cohesive energy of α/γ/fcc |

Table 6: Zirconium Elemental Modified Embedded Atom Method (MEAM) Potential Parameters

| **Elemental Zirconium MEAM Parameters** | **Value** | **Description of Parameter or Source when Fitting** |
|---|---|---|
| lat | BCC | Reference Lattice |
| Ec | 6.2 | Cohesive Energy of α/β |
| α | 4.1 | Bulk modulus of α/β |
| A | 0.48 | Relative stability of α and β |
| $\beta^{(0)}$ | 2.8 | Relative stability of α and β |
| $\beta^{(1)}$ | 2 | Shear elastic constants of α |
| $\beta^{(2)}$ | 7 | Shear elastic constants of α and β |
| $\beta^{(3)}$ | 1 | Shear elastic constants of α and β |
| $t^{(0)}$ | 1 | Set to allow as reference |
| $t^{(1)}$ | 3 | Vacancy formation energy in α and β |
| $t^{(2)}$ | 2 | Shear elastic constants of α and β |
| $t^{(3)}$ | -7 | Atomic volume of α |
| alat | 3.58 | Lattice constant of β |
| $\rho^0$ | 1 | Background Electron Density Scaling |
| attract | 0 | Thermal expansion and stability of β |
| repulse | 0.03 | Thermal expansion and stability of β |
| $C_{min}$ | 0.7 | Cohesive energy of α/β |
| $C_{max}$ | 0.99 | Cohesive energy of α/β |

**Fitting MEAM Potential Parameters**

The bulk modulus and elastic constants can be used to fit the pure element MEAM 1NN potential, then modified for the 2NN MEAM potential. Parameters α, $\beta^{(0)}$ , $\beta^{(2)}$ , and $t^{(2)}$ initial values are set according to the known first principal bulk modulus and elastic constants at zero kelvin by:

$$\alpha = \sqrt{\frac{9B\Omega}{E_c}} \quad (68)$$

$$\beta^{(0)} = \sqrt{\frac{(9B-2Zc\prime)\Omega}{AE_c}} \quad (69)$$

$$\beta^{(2)} = 6 \quad (70)$$

$$t^{(2)} = \sqrt{\frac{Z^2(c_{44}-2c\prime)\Omega}{2AE_c\left(\beta^{(2)}-2\right)^2}} \quad (71)$$

The other parameters are either iterated to fit or directly fitted to experimental and first principal calculations. First principal ground state calculations were performed and experimental data gathered to get a cohesive energy term $E_c$ for both Uranium and Zirconium.

First iteration for both Uranium and Zirconium the other parameters were set to: A=1, $t^{(1)}$=0, $t^{(3)}$=0, $B^{(1)}$=2, $B^{(2)}$=6, $B^{(3)}$=2, Cmin=2.0, Cmax=2.8 and δ=0. Next, A is chosen so that the bcc/fcc and bcc/hcp cohesive energies agree with first principal calculations for uranium and zirconium, respectively. However, when the parameter A is changed, the values for $\beta^{(0)}$ and $t^{(2)}$ change as well. Therefore, this process is iterated until convergence.

The parameter $t^{(3)}$ is changed so that the relaxed stacking fault energy agrees with the first principal calculations. Next, $t^{(1)}$ is changed so that the relaxed vacancy formation energy agrees with the first principal calculations. Then, the $\delta$ parameter is changed so that the thermal expansion coefficient agrees with the experimental value. Then, after the main parameters have been fit the additional parameters like $\beta^{(1)}$, $\beta^{(2)}$, $\beta^{(3)}$, Cmin, Cmax and alat are adjusted to fit the rest of the experimental or first principal values. Finally, all of these steps are repeated and iterated to better fit the experimental or first principal calculation values until a decent agreement is achieved.

Many of the parameter fitting for MEAM described above, assumes only 1NN MEAM fitting, therefore, for fitting a 2NN MEAM many of the starting parameter values can be set to the 1NN MEAM parameters then iterated and adjusted as needed.

FCC was chosen as the reference structure of Uranium because it was relatively simple compared to using a bcc reference structure, where screening parameters are a larger concern. The more complex BCC structure was chosen to be the reference structure of Zirconium to allow the MEAM potential to mimic both hcp and bcc structure behaviors.

The cohesive energy for each element was found through DFT calculations. In addition, DFT calculations were used to calculate the energy differences between phases, as well as the bulk modulus. The bulk modulus of uranium was obtained using the DFT code VASP (Kresse 1993) resulting in 111 GPa for FCC and 121 GPa for BCC uranium. For zirconium, the bulk modulus was found from DFT calculations of HCP and BCC were 83 GPa and 85 GPa, respectively.

Thermal expansion and lattice parameter values were adjusted to match experimental results. The lattice constant is adjusted by changing the "alat" parameter. While the thermal expansion is controlled by the cubic term in the universal equations of state (EOS), commonly referred by δ, is decomposed into two parameters (an attraction and repulsion cubic term parameters). It should also be noted that adjusting the repulsion and attraction parameters can change the melting point.

To obtain the correct thermal expansion values for the elements, each element's repulse=attract MEAM parameters were adjusted, which can also effect the melting point. If the thermal expansion and melting temperature cannot be both fit by adjusting the repulsion and attraction terms it may be necessary to adjust the parameters if you are in a region close to melting. This is very important when the metal transitions into melting or amorphous regions, as is seen when the material is irradiated. When the material is irradiated the metal atoms may have a significant thermal spike around the primary knock on atom (PKA), which could lead to local amorphous regions or melting. This process depends on the energy difference between the bcc and amorphous structures.

**Uranium MEAM vs. First Principals DFT Comparison**

The MEAM parameters were compared against DFT first principal simulations. The first principal DFT calculations were performed in VASP (Kresse 1993), by Dr. Beeler (Beeler 2012a; Beeler, pers. comm.).

It should be noted that Yoo (Yoo 1998) was able to obtain 113GPa experimental bulk modulus for γ BCC Uranium at approximately zero kelvin.

Table 7: Body Centered Cubic (BCC) Uranium Elastic, Bulk modulus and Formation Energy Comparison at Zero Kelvin

| BCC Uranium 0K Elastic Constants, Bulk Modulus and Formation Energy Comparison | | |
|---|---|---|
| **Property** | **MEAM** | **GGA** |
| C11 [Gpa] | 111 | - |
| C12 [Gpa] | 117 | - |
| C44 [Gpa] | 15 | 37 |
| C' [Gpa] | -3 | -35 |
| B [Gpa] | 117 | 121 |
| Vacancy [eV] | 1.34 | 1.38 |
| Interstitial [eV] | 1.8 | 1.54 |

Table 8: Face Centered Cubic (FCC) Uranium Elastic, Bulk modulus and Formation Energy Comparison at Zero Kelvin

| FCC Uranium 0K Elastic Constants and Bulk Modulus Comparison | | |
|---|---|---|
| **Property** | **MEAM** | **GGA** |
| C11 [Gpa] | 91 | - |
| C12 [Gpa] | 129 | - |
| C44 [Gpa] | 20 | 40 |
| C' [Gpa] | -19 | -49 |
| B [Gpa] | 116 | 111 |
| Vacancy [eV] | 1.1 | - |

**Zirconium MEAM vs. First Principals DFT Comparison**

Table 9: Hexagonally Close Packed (HCP) Zirconium Elastic, Bulk modulus and Formation Energy Comparison at Zero Kelvin

| HCP Zirconium 0K Elastic Constants, Bulk Modulus and Formation Energy Comparison | | |
|---|---|---|
| **Property** | **MEAM** | **GGA** |
| C11 [Gpa] | 126 | 144 |
| C33 [Gpa] | 173 | 166 |
| C44 [Gpa] | 23.3 | 33.4 |
| B [Gpa] | 84 | 83 |
| Vacancy [eV] | 1.7 | 1.7 |

Table 10: Body Centered Cubic (BCC) Zirconium Elastic, Bulk modulus and Formation Energy Comparison at Zero Kelvin

| BCC Zirconium 0K Elastic Constants, Bulk Modulus and Formation Energy Comparison | | |
|---|---|---|
| **Property** | **MEAM** | **GGA** |
| C11 [Gpa] | 94 | - |
| C12 [Gpa] | 72 | - |
| C44 [Gpa] | 71 | 34 |
| C' [Gpa] | 11 | -1 |
| B [Gpa] | 81 | 85 |
| Vacancy [eV] | 2.1 | 1.8 |

## Alloy MEAM Parameters

### Alloy MEAM Parameter Fitting

The alloy reference structure chosen for the U-Zr pair potential was B1 for simplicity. Overall, reference crystal structures with first nearest neighbors (1NN) of opposite type are preferred and tend to get better results for most alloys.

First principal calculations, with a B1 crystal structure were used to fit the alloy cohesive energy, lattice constant, energy of the phase, and elastic constants. The alloy MEAM parameters were fit iteratively with a similar procedure as the elemental parameters were. The alloy cohesive energy and reference state equations and calculation methodology for the MEAM alloy can found in the previous Alloy MEAM section. The thermal expansion of the U-Zr alloy is also modified by adjusting the cross elemental cubic attraction and repulsion terms of the EOS.

The elemental parameter “alat” is modified to help the lattice constant and fix the experiential data points of quenched lattice parameters at U-Zr40% and U-Zr90% from Summers-Smith (Summers-Smith 1955). Then, lattice parameters values from Akabori 1995 (Akabori 1995) and Basak 2010 (Basak 2010) were used to verify that they were behaving properly for different temperatures and concentrations.

To fit the MEAM enthalpy of mixing curve to the first principal enthalpy of mixing curve for ground state U-Zr solution by Landa (Landa 2009), the alloy screening

parameters had to be adjusted. These screening parameters were fit iteratively using the enthalpy of mixing of the MS-MC simulation and analyzing ordering behaviors.

Table 11: Alloy Modified Embedded Atom Method (MEAM) Potential Parameters

| **Alloy (U-Zr) MEAM Parameter** | **Value** | **Description of Parameter / How was Fit** |
|---|---|---|
| Lattice | B1 | Reference Lattice Structure |
| $r_e$ | 2.85 | Equilibrium Lattice Constant for B1 Reference Structure |
| $\Delta$ | 0.7 | Change of Cohesive Energy when Mixing, fit to Enthalpy of Mixing |
| $\alpha$ | 5.5 | Bulk Modulus of B1 Reference Structure |
| rcut | 5.5 | Cut-Off Distance |
| xncut | 2 | Power term in cut-off function, fit to match stacking fault energy |
| xmcut | 6 | Power term in cut-off function, fit to match stacking fault energy |
| $\delta$ (attract=repulse) | 0.4 | Thermal Expansion of U-Zr |

Table 12: Binary Alloy Modified Embedded Atom Method (MEAM) Potential Screening Parameters

| **Parameter** | **U-U-U** | **U-Zr-U** | **Zr-U-U** | **Zr-Zr-U** | **Zr-U-Zr** | **Zr-Zr-Zr** |
|---|---|---|---|---|---|---|
| Cmax | 1.7 | 2.8 | 2.8 | 2.8 | 2.8 | 0.99 |
| Cmin | 1.2 | 0.6 | 0.8 | 0.8 | 0.6 | 0.7 |

The theory and fitting procedure of a second-nearest neighbor MEAM potential can be found in publications by Byeong-Joo Lee and M. I. Baskes (Lee 2000; Lee 2001). Most of the elemental parameters are chosen to match experimental, *ab-initio*, or Density Functional Theory (DFT) values (Baskes 1992; Baskes 1999), while the many of the alloy parameters are obtained through trial and error processes.

## Limitations of This MEAM Potential

The MEAM potential used has some unresolved problems, and is unable to replicate the U-Zr alloy over all concentrations and temperatures. One of the regions that the MEAM potential is unable to replicate is the high temperature range, 800K and above, for the uranium-rich U-Zr alloy with 30 atomic percent Zirconium or less. In this region the BCC phase is unstable when the uranium and zirconium atoms are mixed.

In addition, the experimental ordering and enthalpy of mixing at higher temperatures, 1000K and above, shows a drastically different trend than the first principal calculations or this MEAM potential MD simulations. To match the experimental results at higher temperatures, a new MEAM potential will have to be formed.

## Molecular Statics (MS) and Monte Carlo (MC) Simulations

The MEAM potential used in the simulations results in good agreement with the *ab-initio* and CALPHAD heat of mixing curves from Landa et al. (Landa 2009). The positive heat of mixing suggests the possible existence of a miscibility gap in the U-Zr phase diagram using the MEAM potential.

The maximum heat of mixing from the MS-MC simulation around $U_{60}Zr_{40}$ is close to the first principals estimated maximum between $U_{70}Zr_{30}$ and $U_{60}Zr_{40}$ (Landa 2009).

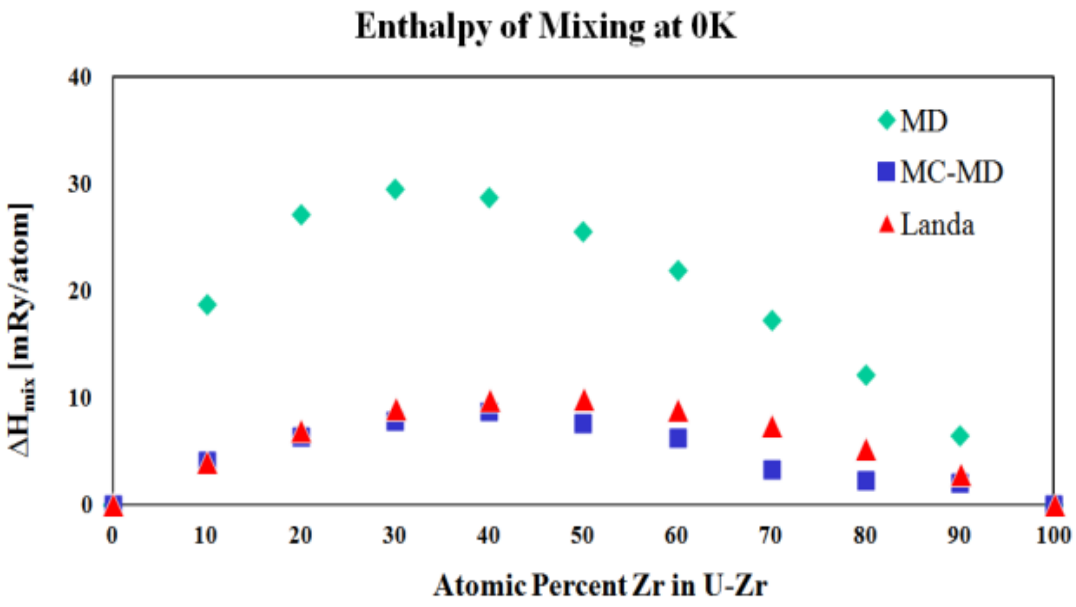


Figure 24: Comparison of the Enthalpy of Mixing (Formation Energy) at Zero Kelvin

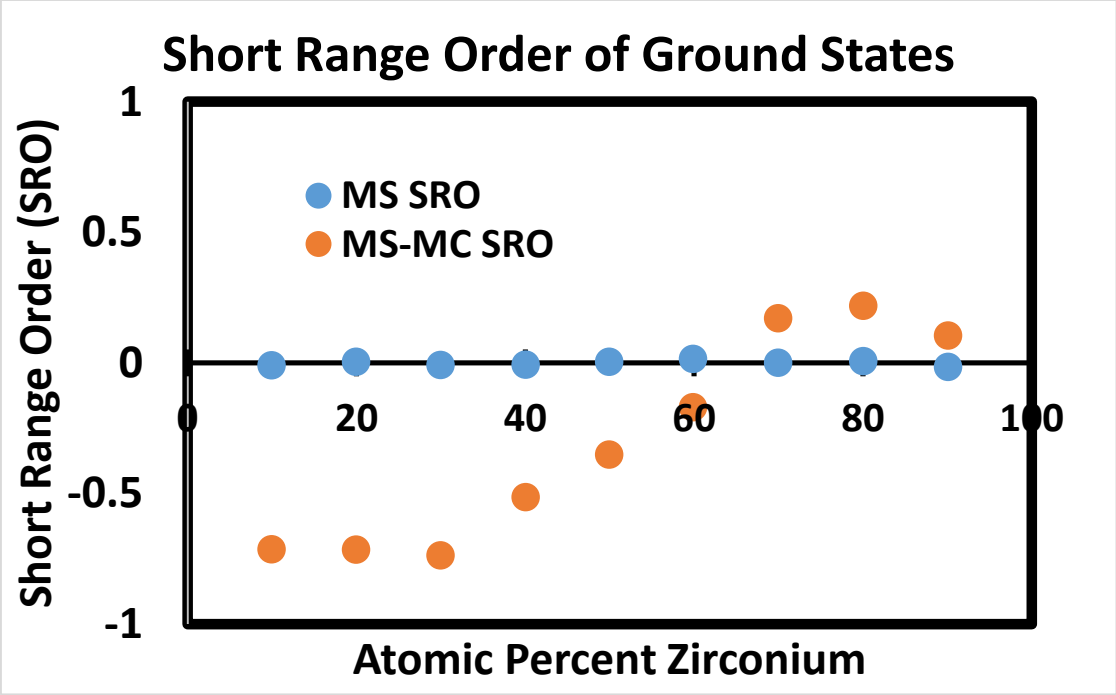


Figure 25: Short Range Order (SRO) of the Ground States with Varying Composition after MS-MC iterations were performed

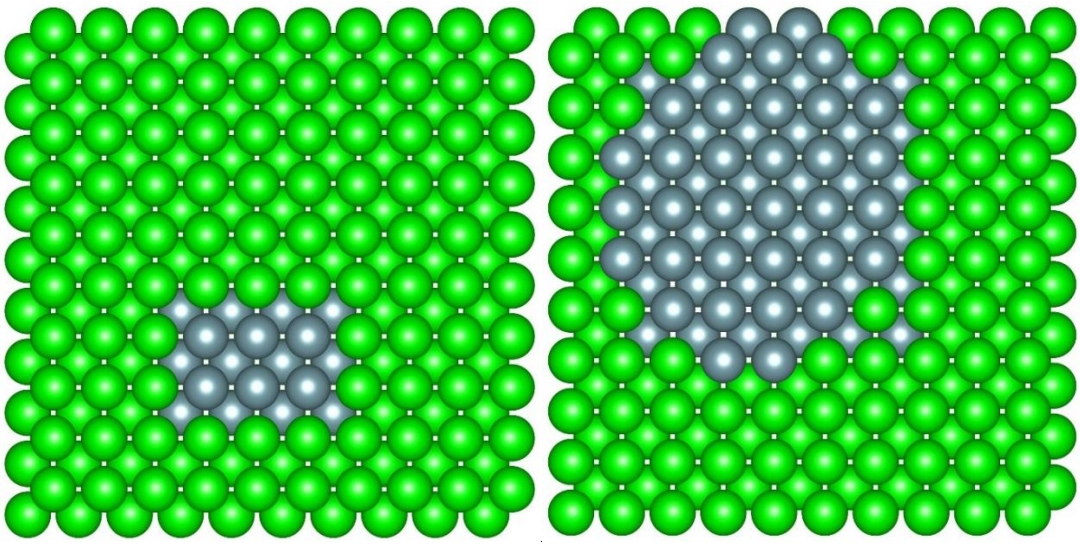

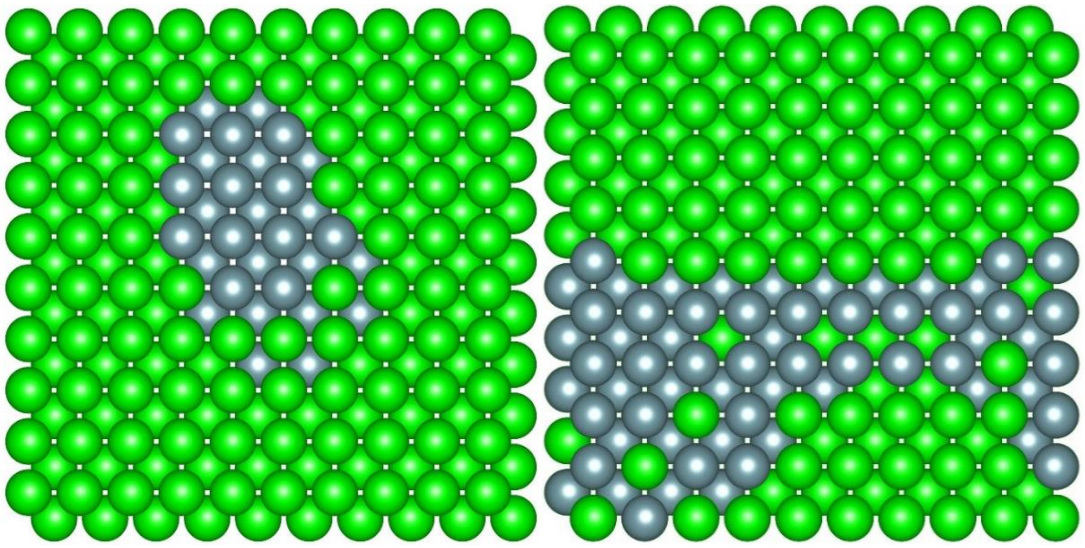

**(c)** **(d)**

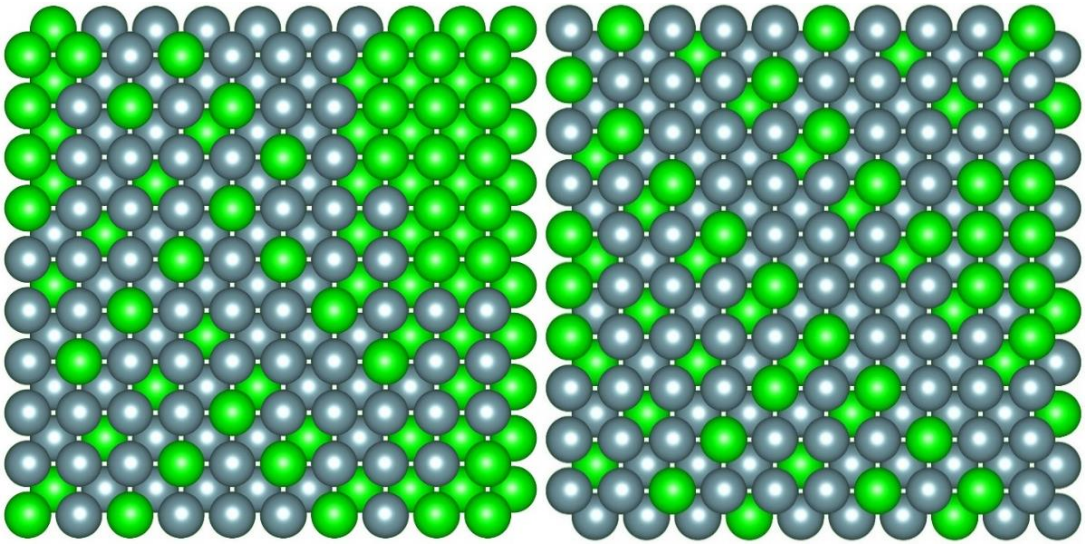

**(e)** **(f)**

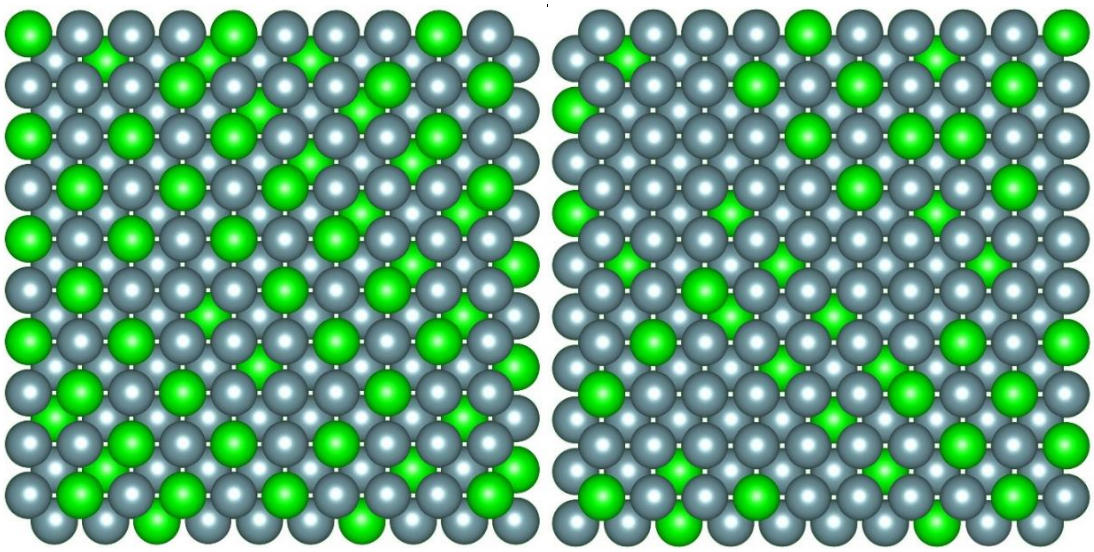

**(g)** **(h)**

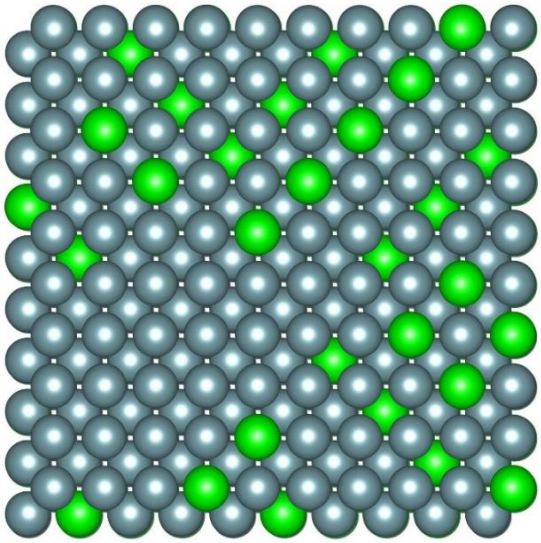

**(i)**

Figure 26: Snap-Shots of the Atom Configurations at the Ground State for Various U-Zr Alloy Concentrations after MS-MC Simulation Iterations (a) γ-$U_{90}Zr_{10}$ (b) γ-$U_{80}Zr_{20}$ (c) γ-$U_{70}Zr_{30}$ (d) γ-$U_{60}Zr_{40}$ (e) γ-$U_{50}Zr_{50}$ (f) γ-$U_{40}Zr_{60}$ (g) γ-$U_{30}Zr_{70}$ (h) γ-$U_{20}Zr_{80}$ (i) γ-$U_{10}Zr_{90}$

## Transition to the Delta U-Zr Phase

The transition from the body centered cubic to the delta phase of U-Zr has been explained by Dr. Basak (Basak 2010; Basak 2011) to be an omega transformation mechanism in which alternate (111) planes of the U-Zr BCC phase (parent phase) collapse to form $AlB_2$ type hexagonal crystal structure. The ordering in Figures 27, 28 and 29 below show atoms arranging themselves in alternating (111) planes, showing the thermodynamic push for the atoms to arrange themselves in the beginning stages of the gamma (bcc) to delta (C32) U-Zr phase.


Figure 27: U-Zr70 (70 Atomic Percent Zirconium), Snap-shot of Atomic Configurations in the Ground State Viewed from the [110] direction After the MS-MC Simulation Iterations

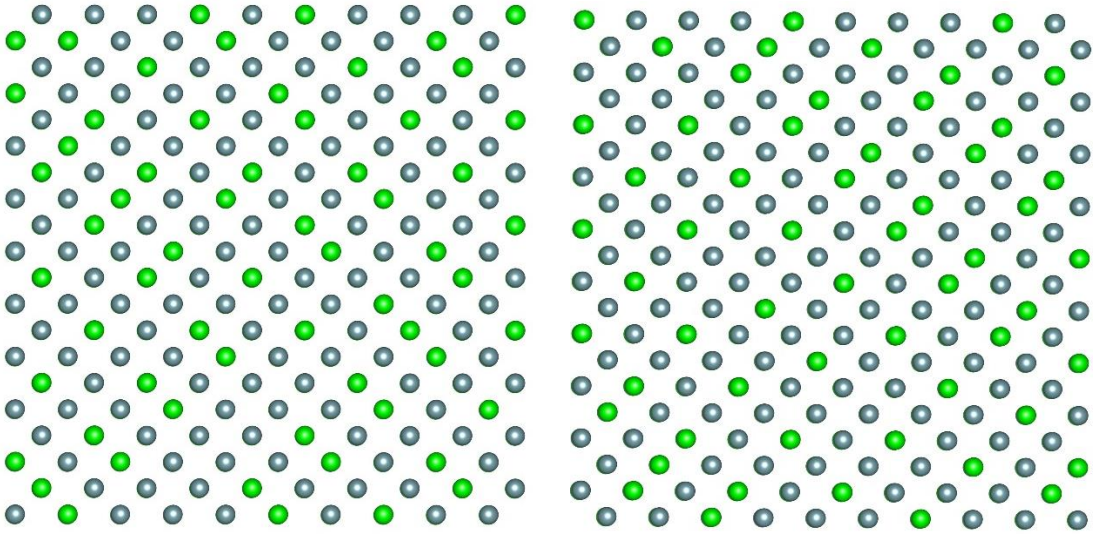

Figure 28: U-Zr70 (70 Atomic Percent Zirconium), Snap Shot of Atomic Configuration viewed from the [100] direction after the MS-MC iterative simulations

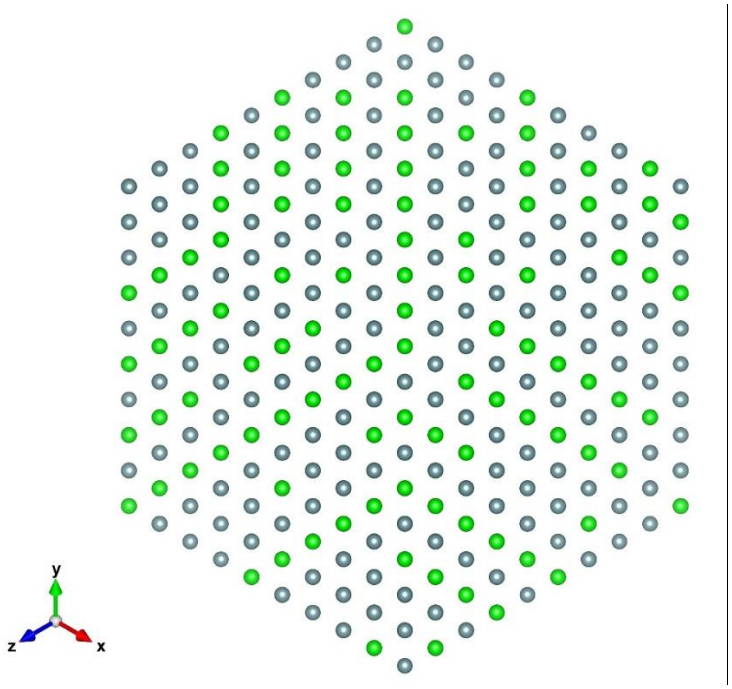


Figure 29: U-Zr70 (70 Atomic Percent Zirconium), Snap Shot of Atomic Configuration viewed from the [111] direction after the MS-MC Iterative Simulations

**Molecular Dynamics (MD) and Monte Carlo (MC) Simulations**

The Molecular Dynamics Simulation for a random solid solution lattice parameter (which can be used to approximate the thermal expansion) is in agreement with the experimental lattice parameter value for γ-$U_{30}Zr_{70}$ alloy, within a few percent. The experimental lattice parameter from Landa et al. is 3.589Å for γ-$U_{30}Zr_{70}$ alloy at the γ-δ transition temperature T=925K (Akabori 1995), while the MD simulation lattice parameter was 3.5467Å.

The thermal expansion of the Molecular Dynamics Simulation results in the expected linear curve seen below in Figure 30, while the MC-MD thermal expansion has a non-linear nature corresponding to the ordering of the system.

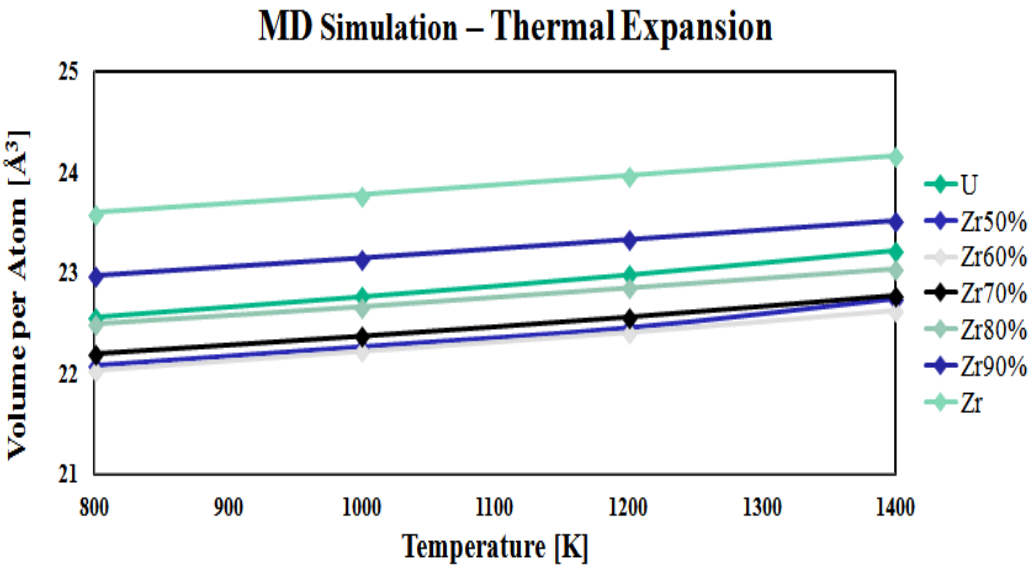


Figure 30: Thermal Expansion from Molecular Dynamics Simulation of a Random Solid Solution (Moore 2013)

The thermal expansion and additional properties for pure Uranium given this MEAM potential were reported by Dr. Beeler (Beeler 2012b).

Table 13: The melting temperature, enthalpy of fusion, volume change on melting, specific heat capacity and thermal expansion are calculated and compared to experimental values (Beeler 2012b)

| Property | MEAM Value | Experimental Value |
|---|---|---|
| $T_{melt}$ (K) | 1410 | 1408 |
| $\Delta H_{fusion}$ (kJ $mol^{-1}$) | 8.66 | 8.5 |
| $\Delta V_{melt}$ (%) | 2.17 | - |
| $C_p$ (J $g^{-1}$ $K^{-1}$) | 0.11 | 0.12 |
| Linear Volume Coefficient of Thermal Expansion (per 100 K) | 0.19% | 0.22% |

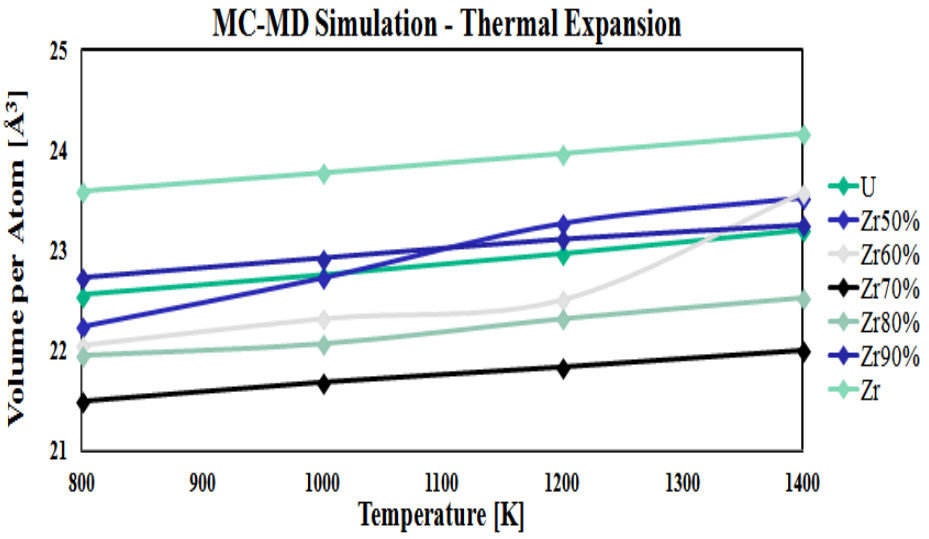


Figure 31: Thermal Expansion from Iterative Molecular Dynamics and Monte Carlo (Moore 2013)

## Separation (Order/Disorder)

The results of the Molecular Dynamics (MD) simulation against the iterative Monte Carlo and Molecular Dynamics (MC-MD) simulation relate the difference in properties from a random solid solution versus an ordered or disordered system. Real solutions cannot always be assumed to be random. Real solutions tend to an atomic arrangement that minimizes the free energy of the mixture.

The order/disorder of the system was seen to play a role in phase stability. In some cases for higher temperature simulations, the order/disorder transition of the atoms improved the stability of the BCC crystal phase where a MD simulation on a random solid solution would have melted.

Forced symmetry was enforced on the periodic lattice, resulting in the $\gamma$ to $\delta$ phase transition of the Uranium-Zirconium alloy remaining in a Body Centered Cubic Crystal structure. The $\gamma$ to $\delta$ phase transition for U-Zr can still be observed through the ordering of the MC-MD simulation when finding the low energy structure.

The lowest energy structure around 50% Zirconium should be disordered, which is replicated by the MEAM potential. Experimentally, an ordered C32 structure is seen around 67% Zirconium. Therefore we expect an ordered structure to form during the MC-MD simulations. This is also replicated by the MEAM potential. The MC-MD simulation result at 60% Zirconium is separated while the 70% Zirconium ordering begins to occur. Figure 32 below shows that clustering begins to occur for U-Zr at sixty atomic percent zirconium. In addition, the figure shows separation by fifty atomic percent zirconium.

The iterative Monte Carlo and Molecular Dynamics simulations were run at 800 kelvin for an array of atomic compositions of Uranium-Zirconium alloy consisting of 2000 periodic atoms. The final atomic configuration seen in Figure 32 clearly shows the preferential atomic ordering for each composition of Uranium and Zirconium atoms.

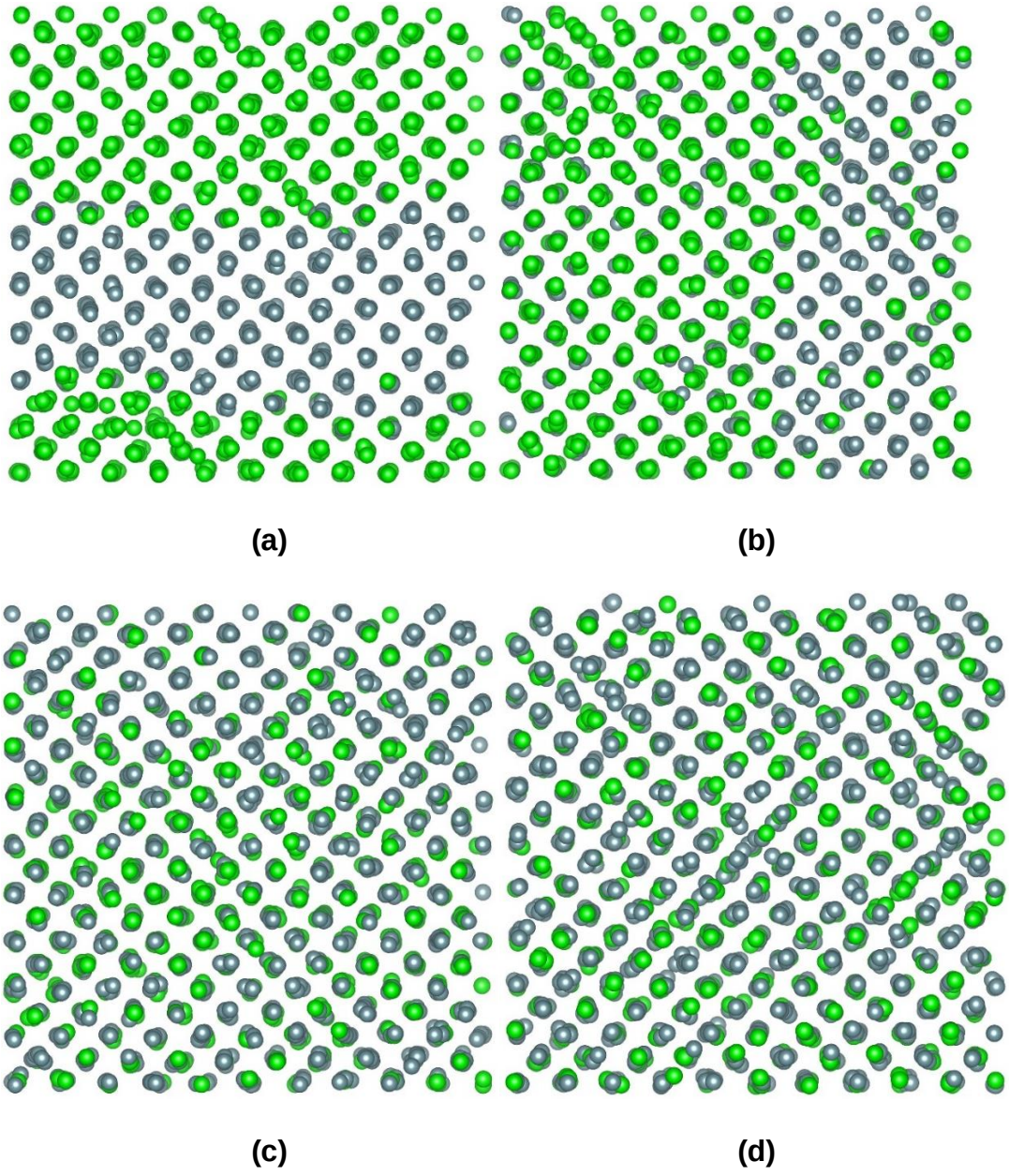

**(a)** **(b)**

**(c)** **(d)**

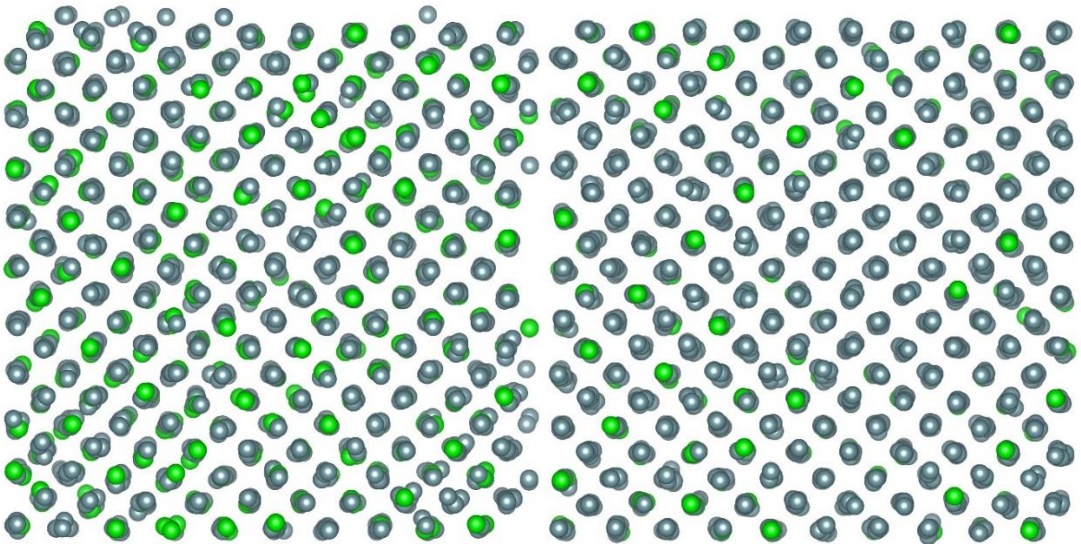

**(e)** **(f)**

Figure 32: Atomic Arrangements after the Completion of the Iterative Molecular Dynamics and Monte Carlo Simulations at 800K for (a) γ-$U_{60}Zr_{40}$ (b) γ-$U_{50}Zr_{50}$ (c) γ-$U_{40}Zr_{60}$ (d) γ-$U_{30}Zr_{70}$ (e) γ-$U_{20}Zr_{80}$ (f) γ-$U_{10}Zr_{90}$ (Moore 2013)

The short-range order (SRO) parameter is a measure of the order versus disorder of the alloy system, once again showing the clustering to segregation effect of U-Zr for lower Zirconium concentrations and the ordering for higher Zirconium concentrations.

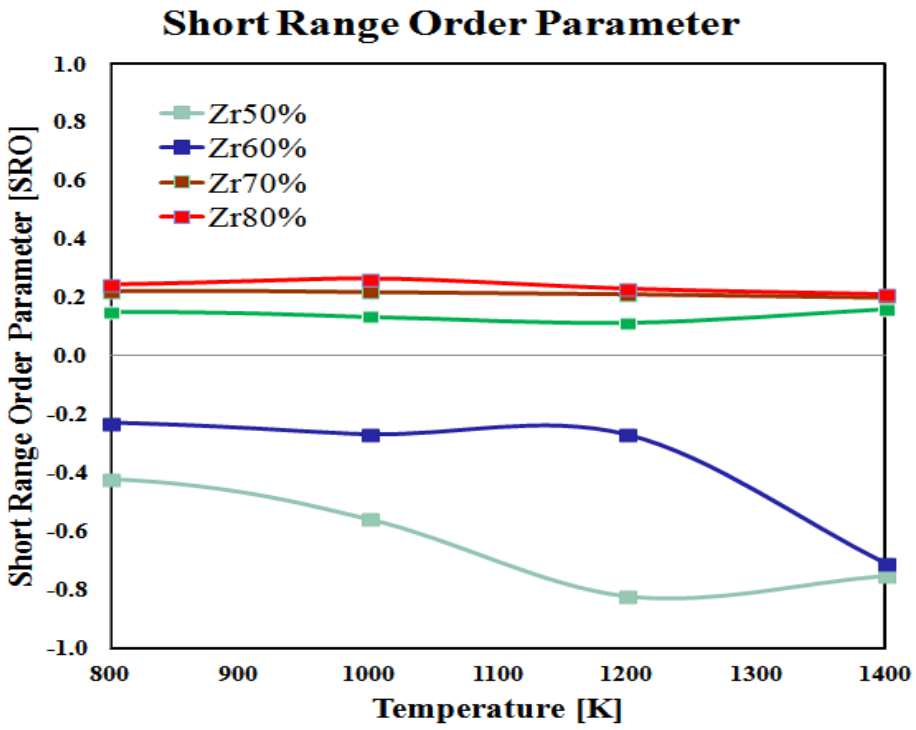


Figure 33: Short Range Order Parameter for Various Atomic Percent Zirconium in the Uranium-Zirconium Alloy (Moore 2013)

It is important to remember that the SRO magnitudes will decrease as the concentration moves away from 50-50%.

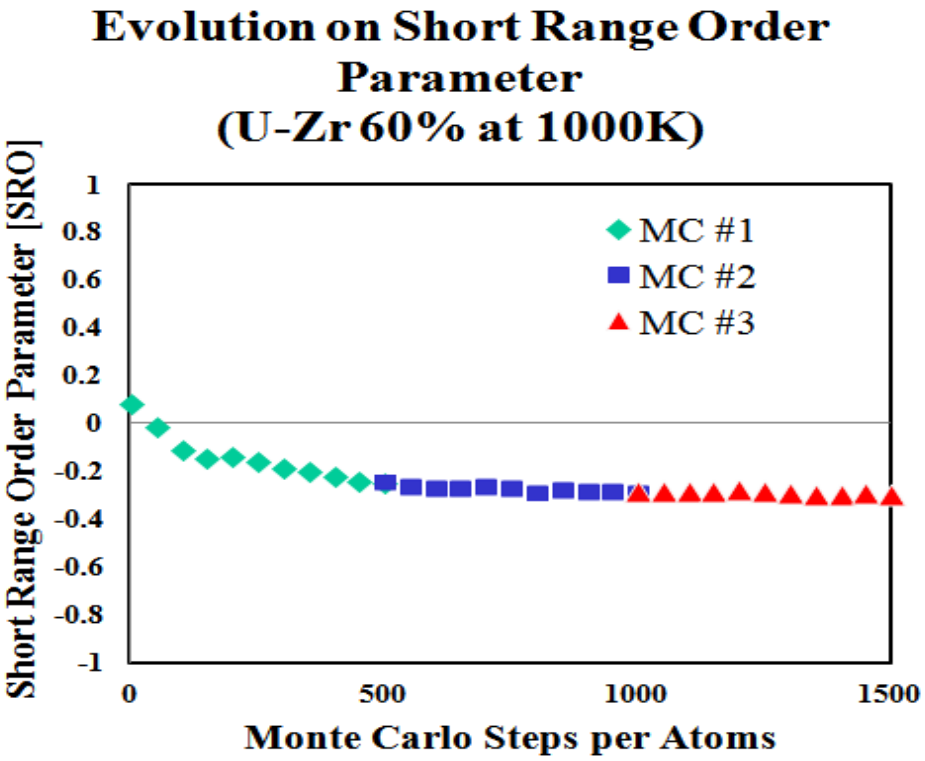


Figure 34: Short Range Order Parameter Evolution throughout the Iterative Molecular Dynamics and Monte Carlo Simulations (Moore 2013)

The short-range order in Figure 34 shows that the MEAM potential used in the MC-MD simulations at lower temperatures captures the expected physical ordering. However, at higher temperatures, $U_{50}Zr_{50}$ and $U_{40}Zr_{60}$ differ from the expected ordering. Around approximately 950K, both $U_{50}Zr_{50}$ and $U_{40}Zr_{60}$ should approach a more random solution.

**Separation in Uranium-Rich U-Zr Alloy**

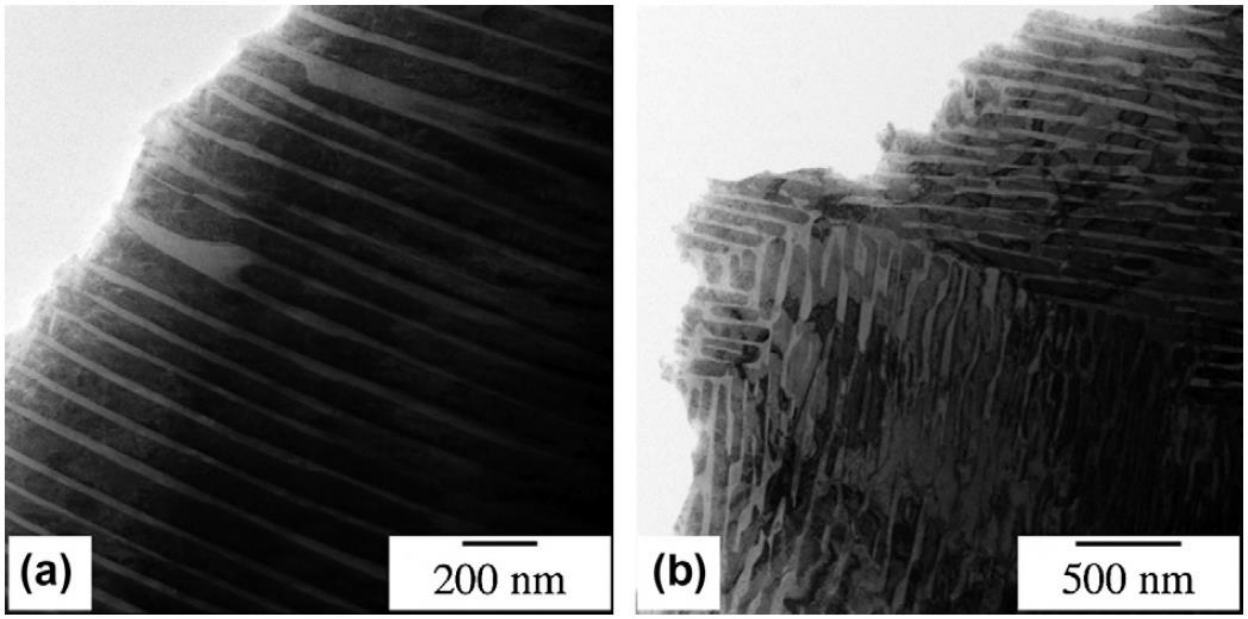


Figure 35: (a, b) Bright-field TEM images of the as-cast U-10Zr (Zirconium 10% by weight, corresponding to approximate 23 atomic percent) alloy showing alternating lamella, with adjacent variants of the lamellar structure evident in (b) (McKeown 2013)

A uranium rich U-Zr alloy of 10% wt. Zirconium was produced by met-casting. The sample was heated at a rate of 50°/min to approximately 1900°C, which is above the melting temperature. Then is was held isothermal for 1 hour before cooling back down to room temperature at a rate of 30°/min. Then the sample was flipped and the process was repeated. (McKeown 2013)

This separation effect can also be seen in the MEAM potential. At 800K, while the potential is unstable for alloys with a zirconium concentration under thirty atomic percent, we can see that under U-Zr50 at. % (in Figure 32 (a) and (b)) there is a separation resulting in bands of Uranium and Zirconium. These separation bands mimic the separation seen in the TEM image. The as-cast fuel shown in the TEM image is of

similar concentration to the MEAM MD simulation showing the band separation. This indicates that the MEAM potential, even though held in the BCC phase, mimics the thermodynamic push toward separation for uranium-rich U-Zr.

It should be noted that the separation behavior at zero kelvin (MS-MC) differs from the separation behavior witnessed in the temperature (MD-MC) simulations. The zero kelvin simulations result in a clustering behavior in the uranium rich alloys (Figure 26 (a, b, c, d, e)), while the simulations at 800K results in a more band-like separation ( Figure 32 (a, b)).

# CHAPTER 5

## SUMMARY and CONCLUSIONS

Recently, there has been renewed research into uranium nuclear metallic alloys. However, previous research on the principals of the thermodynamic properties and atomistic ordering is limited, despite the complex ordering phenomenon observed for metallic fuels. This work uses a Modified Embedded Atom Method (MEAM) interatomic potential fit to first principal and experimental values to analyze ordering phenomenon in the body centered cubic (BCC) phase of interest. One of the benefits of creating a MEAM potential for this analysis, is that it can be used to analyze large atomic systems at high temperature, which cannot be accomplished using first principal methodology due to computational run time restrictions. The U-Zr MEAM potential is the first interatomic potential that has been created for the U-Zr metallic alloy.

The Modified Embedded Atom Method (MEAM) potential results in replicating both the δ-γ phase transitions, the uranium-rich separation and the thermal expansion of the Uranium-Zirconium alloy. In addition, the MEAM potential results in agreement with the first principals Heat of Formation Curve (Enthalpy of Mixing) and ordering at 0K – 1000K. However, the MEAM potential is limited to the moderate to high zirconium concentration for the Uranium-Zirconium alloy.

Comparing the zero kelvin (MS-MC) simulations against the temperature (MD-MC) simulations in uranium-rich U-Zr alloys, a clustering versus band like separation is

seen. This leads us to believe that the band like separation seen in as-cast uranium-rich U-Zr alloys is due to a thermodynamic push at temperature.

While the MEAM potential is able to capture many of the U-Zr properties, a few scenarios still need work. The MEAM potential must be adjusted to accurately capture ordering effects at higher temperatures and to capture the body centered cubic stability for low atomic percent zirconium. In addition, the experimental ordering and enthalpy of mixing at higher temperatures shows a drastically different trend than the first principal calculations or this MEAM potential MD simulations. To match the experimental results at higher temperatures, a new MEAM potential will have to be formed.

Uranium-Zirconium metal alloy fuels have a promising future in nuclear science. With the MEAM potential used in Molecular Dynamics (MD) and Monte Carlo (MC) simulations, the phases and properties of the U-Zr alloy can be accurately reproduced. This is a large step in understanding fundamental properties of metallic nuclear fuels and developing a computational model for use in a fuel performance code.

# REFERENCES


Akabori, M., et al. "Stability and structure of the d phase of the U-Zr alloys. "Journal of nuclear materials 188 (1992): 249-254.

Akabori, Mitsuo, et al. "The lattice stability and structure of delta-UZr2 at elevated temperatures." Journal of Physics: Condensed Matter 7.43 (1995): 8249.

Alex P. Moore, Ben Beeler, Michael Baskes, Maria Okuniewski and Chaitanya S. Deo (2013). Atomistic Ordering in Body Centered Cubic Uranium-Zirconium Alloy. MRS Proceedings, 1514, mrsf12-1514-hh11-08 doi:10.1557/opl.2013.517.

Basak, C. B., et al. "Disordered bcc γ-phase to δ-phase transformation in Zr-rich U-Zr alloy." Philosophical Magazine 91.24 (2011): 3290-3306.

Basak, Chandra Bhanu, N. Prabhu, and Madangopal Krishnan. "On the formation mechanism of UZr2 phase." Intermetalics 18.9 (2010): 1707-1712.

Baskes, ATOMISTIC MODELS OF METALS AND ALLOYS FOR NUCLEAR ENERGY APPLICATIONS, un-published presentation on December 5th & 7th 2011 at Georgia Institute of Technology

Baskes, M. I. "Modified embedded-atom potentials for cubic materials and impurities." Physical Review B 46.5 (1992): 2727.

Baskes, M. I., and R. A. Johnson. "Modified embedded atom potentials for HCP metals." Modelling and Simulation in Materials Science and Engineering 2.1 (1999): 147.

Bauer, A. A. (1959). An Evaluation of the Properties and Behavior of Zirconium-Uranium Alloys, Battelle Memorial Inst., Columbus, Ohio.

Beeler, B., et al. (2010). "First principles calculations for defects in U." Journal of Physics: Condensed Matter 22(50): 505703.

Beeler, B., et al. (2011). "First-principles calculations of the stability and incorporation of helium, xenon and krypton in uranium." Journal of Nuclear Materials.

Beeler, Benjamin, et al. "Atomistic properties of γ uranium." Journal of Physics: Condensed Matter 24.7 (2012b): 075401.

Beeler, Benjamin, et al. "First principles calculations of the structure and elastic constants of a, ß and γ uranium." Journal of Nuclear Materials (2012a).

Born M, Huang K (1954) Dynamical theory of crystal lattices. Clarendon Press, Oxford, 420 pp

Bozzolo, G., et al. (2010). "Surface properties, thermal expansion, and segregation in the U–Zr solid solution." Computational Materials Science 50(2): 447-453.

C.S. Yoo, H. Cynn, P. Soderlind, Physical Review B, 57 (1998) 10359-10362

Carmack, Jon, and Kemal Pasamehmetoglu. Options Study Documenting the Fast Reactor Fuels Innovative Design Activity. No. INL/EXT-10-19999. Idaho National Laboratory (INL), 2010.

Chevalier, Pierre-Yves, Evelyne Fischer, and Bertrand Cheynet. "Progress in the thermodynamic modelling of the O–U–Zr ternary system." Calphad 28.1 (2004): 15-40.

Cui, Zhiwei, et al. "Developing a second nearest-neighbor modified embedded atom method interatomic potential for lithium." Modelling and simulation in materials science and engineering 20.1 (2012): 015014.

D.R. Olander, Fundamental Aspects of Nuclear Reactor Elements, ERDA, Springfield, VA, 1975

Droegkamp, R. (1955). HOT MALLEABILITY OF ZIRCALOY-2 AND HIGH ZIRCONIUM-URANIUM ALLOYS, Westinghouse Electric Corp. Atomic Power Div., Pittsburgh.

Evans, Denis J., and Brad Lee Holian. "The nose–hoover thermostat." The Journal of chemical physics 83 (1985): 4069.

Hofman, G. L., S. L. Hayes, and M. C. Petri. "Temperature gradient driven constituent redistribution in U-Zr alloys." Journal of nuclear materials 227.3 (1996): 277-286.

Hünenberger, Philippe H. "Thermostat algorithms for molecular dynamics simulations." Advanced Computer Simulation. Springer Berlin Heidelberg, 2005. 105-149.

Inhomogeneous Electron Gas, P. Hohenberg and W. Kohn, Phys. Rev. 136, B864 (1964).

J.H. Rose, J.R. Smith, F. Guinea, and J. Ferrante, Phys. Rev. B 29, 2963 (1984)

Jaric, Jovo P., Dragoslav Kuzmanovic, and Zoran Golubovic. "On tensors of elasticity." Theoretical and Applied Mechanics 35.1-3 (2008): 119-136.

Jelinek, B., et al. "Modified embedded atom method potential for Al, Si, Mg, Cu, and Fe alloys." Physical Review B 85.24 (2012): 245102.

Jelinek, B., et al. "Modified embedded-atom method interatomic potentials for the Mg-Al alloy system." Physical Review B 75.5 (2007): 054106.

Kim, Young-Min, Byeong-Joo Lee, and M. I. Baskes. "Modified embedded-atom method interatomic potentials for Ti and Zr." Physical Review B 74.1 (2006): 014101.

Kittel, J. H., et al. "History of fast reactor fuel development." Journal of nuclear materials 204 (1993): 1-13.

L.C. Walters, B.R. Seidel and J.H. Kittel, Nucl. Technol. 65 (1984) 179

Landa, A., et al. (2012). "Ab Initio Study of Advanced Metallic Nuclear Fuels for Fast Breeder Reactors." MRS Online Proceedings Library 1444(1).

Landa, Alex, Per Söderlind, and Patrice EA Turchi. "Density-functional study of the U–Zr system." Journal of Alloys and Compounds 478.1 (2009): 103-110.

Ledbetter, H. M., and Richard Palmer Reed. "Elastic Properties of Metals and Alloys, I. Iron, Nickel, and Iron-Nickel Alloys." Journal of Physical and Chemical Reference Data 2 (1973): 531.

Lee B J 2007 A modified embedded atom method interatomic potential for silicon Calphad 31 95–104

Lee, Byeong-Joo, and M. I. Baskes. "Second nearest-neighbor modified embedded-atom-method potential." Physical Review B 62.13 (2000): 8564.

Lee, Byeong-Joo, et al. "Second nearest-neighbor modified embedded atom method potentials for bcc transition metals." Physical Review B 64.18 (2001): 184102.

Leibowitz, L., et al. (1989). "Thermodynamics of the uranium-zirconium system." Journal of Nuclear Materials 167: 76-81.

Li, Yan, and R. Bruce Thompson. "Relations between elastic constants Cij and texture parameters for hexagonal materials." Journal of applied physics 67.5 (1990): 2663-2665.

Li, Yangzhong, et al. "Classical interatomic potential for orthorhombic uranium."Journal of Physics: Condensed Matter 24.23 (2012): 235403.

Malone, James, et al. "Lightbridge Corporation's Advanced Metallic Fuel for Light Water Reactors." Nuclear technology 180.3 (2012): 437-442.

Matter, H., J. Winter, and W. Triftshäuser. "Investigation of vacancy formation and phase transformations in uranium by positron annihilation." Journal of Nuclear Materials 88.2 (1980): 273-278.

McKeown, J. T., et al. “Coexistence of the α and δ phases in as-cast uranium-rich U-Zr alloy.” Journal of Nuclear Materials (2013).

Metropolis N, Rosenbluth A W, Rosenbluth M N, Teller A H and Teller A E 1953 J. Chem. Phys. 21 1087

Moore, Alex P., et al. "Atomistic Ordering in Body Centered Cubic Uranium-Zirconium Alloy." MRS Proceedings. Vol. 1514. Cambridge University Press, 2013 .

Ogata, Takanari, et al. "Analytical study on deformation and fission gas behavior of metallic fast reactor fuel." Journal of nuclear materials 230.2 (1996): 129-139.

Ogata, Takanari, et al. "Reactions between U–Zr alloys and Fe at 923 K." Journal of nuclear materials 250.2 (1997): 171-175.

Okamoto, H. (2007). "U-Zr (Uranium-Zirconium)." Journal of Phase Equilibria and Diffusion 28(5): 499-500.

Ondracek, Gerhard, and Brigitte Schulz. "The porosity dependence of the thermal conductivity for nuclear fuels." Journal of Nuclear Materials 46.3 (1973): 253-258.

P. Soderlind, Advances in Physics, 47 (1998) 959-998

Package, Vienna Ab-initio Simulation. "G. Kresse and J. Hafner." Phys. Rev. B 47 (1993): 558.

Pahl, Porter, Crawford and Walters Irradiation behavior of metallic fast reactor fuels, Journal of Nuclear Materials 188 (1992) 3-9

Pahl, R. G., et al. "Experimental studies of U-Pu-Zr fast reactor fuel pins in the experimental breeder reactor-ll." Metallurgical Transactions A 21.7 (1990): 1863-1870.

Personal Communication with Dr. Beeler and Dr. Baskes.

Rose, Smith, Ferrante, Phys Rev. B 28, 1835 (1983)

Rough, F. (1955). An Evaluation of Data on Zirconium-Uranium Alloys, Battelle Memorial Inst., Columbus, Ohio.

Self-Consistent Equations Including Exchange and Correlation Effects, W. Kohn and L.J. Sham, Phys. Rev. 140, A1133 (1965).

Skinner, Gordon B., and Herrick L. Johnston. THERMAL EXPANSION OF ZIRCONIUM BETWEEN 298 AND 1600 K. No. 280-9. OHIO STATE UNIV RESEARCH FOUNDATION COLUMBUS CRYOGENIC LAB, 1953.

Smirnova, D. E., S. V. Starikov, and V. V. Stegailov. "Interatomic potential for uranium in a wide range of pressures and temperatures." Journal of Physics: Condensed Matter 24.1 (2012): 015702.

Steven L. Hayes and Douglas L. Porter, Fast Reactor Fuels, Nuclear Fuels and Materials Division Fuel Performance and Design Department, June 5, 2009

Summers-Smith, D. "The Constitution of Uranium-Zirconium Alloys." J. Inst. Metals 83 (1955).

Tromans, Desmond. "Elastic anisotropy of HCP metal crystals and polycrystals." Department of Materials Engineering, University of British Columbia, Vancouver BC, Canada (2011).

W. M. Stacey, et al., "Resolution of Fission and Fusion Technology Integration Issues: An Upgraded Design Concept for the Subcritical Advanced Burner Reactor (SABR)", Nuclear Technology (to be published).

Wang, Guofeng, et al. "Quantitative prediction of surface segregation in bimetallic Pt–M alloy nanoparticles (M= Ni, Re, Mo)." Progress in surface science 79.1 (2005): 28-45.

Y.S. Kim, G.L. Hofman, S.L. Hayes, Y.H. Sohn, J. Nuc. Mat. 327 (2004) 27-36.

Yakel, Harry L. Review of x-ray diffraction studies in uranium alloys. No. CONF-740205--9. Oak Ridge National Lab., Tenn. (USA), 1973.

Yoo C, Cynn H and Soderlind P 1998 Phys. Rev. B 57 10359

Zener, Clarence. Elasticity and anelasticity of metals. University of Chicago press, 1948.

“Hexagonal Closed Packing HCP”, picture png, accessed 8/20/2013, http://biochem.co/2008/08/close-packing-metallic-elements/

“AlB2 Omega Structure”, picture jpg, accessed 8/20/2013, OHBA’s Laboratory HP, http://www.geocities.jp/ohba_lab_ob_page/structure6.html